이학박사 학위논문

Preclinical modeling of Osimertinib for Epidermal Growth Factor Receptor Exon 20 Insertion Mutant Non-Small Cell Lung Cancer

상피성장인자수용체 엑손 20 삽입 돌연변이 비소세포폐암 세포주에서 osimertinib 효능예측 연구

2020 년 2 월

서울대학교 대학원

협동과정 종양생물학전공

이 유 수

A Thesis of the Degree of Doctor of Philosophy

상피성장인자수용체 엑손 20 삽입 돌연변이 비소세포폐암 세포주에서 osimertinib 효능예측 연구

Preclinical Modeling of Osimertinib for Epidermal Growth Factor Receptor Exon 20 Insertion Mutant Non-Small Cell Lung Cancer

February 2020

The Department of Cancer biology,
Seoul National University
College of Medicine
Yusoo Lee

ABSTRACT

이 유 수 (Yusoo Lee)
종양생물학과 (Cancer biology)
The Graduate School
Seoul National University

Introduction: Non-small cell lung cancer (NSCLC) with epidermal growth factor receptor (*EGFR*) exon 20 insertion mutations is the third most common type of *EGFR*-mutant NSCLC and is resistant to EGFR tyrosine kinase inhibitors (TKIs). This study was conducted to evaluate the efficacies of the 1st- to the 3rd-generation EGFR TKIs against NSCLC cells harboring *EGFR* exon 20 insertion mutations.

Methods: We developed seven *EGFR* exon 20 insertion-mutant Ba/F3 models using site-directed mutagenesis and one patient-derived NSCLC cell line (SNU-3173) of subtypes A763insFQEA, V769insASV, D770insSVD, D770insNPG, P772insPR, H773insH, H773insNPH, and H773insAH. Cell viability assays, immunoblotting, and N-Ethyl-N-nitrosourea (ENU) mutagenesis screenings were performed. *EGFR* exon 20 insertion-mutant structures and couplings with osimertinib, a 3rd-generation EGFR TKI, were modeled and compared.

Results: *EGFR* exon 20 insertion-mutant NSCLC cells, excluding *EGFR* A763insFQEA, were resistant to the 1st-generation EGFR TKIs (IC_{50},

1.1±0.067 to 5.4±0.115 μM). Mutants were sensitive to the 2nd-generation EGFR TKIs (IC_{50}, 0.02±0.0002 to 161.8±18.7nM), except *EGFR* H773insH (IC_{50}, 46.3±8.0 to 352.5±22.7nM). The IC_{50} ratios for mutant to wild-type cells were higher than those for the 3rd-generation EGFR TKIs. The 3rd-generation EGFR TKI osimertinib was highly potent against *EGFR* exon 20 insertion-mutant cells (IC_{50}, 14.7 to 62.7nM), including *EGFR* H773insH, and spared wild-type *EGFR* cells. Flexible binding aspect of osimertinib to EGFR exon 20 insertion mutants was revealed through homology modeling and docking simulations. ENU mutagenesis screening of *EGFR* exon 20 insertion-mutant Ba/F3 cells showed various second sites for *EGFR* mutations, mostly in exons 20 and 21, including E762K, P794S, and G796D. In addition, osimertinib-resistant SNU-3173 cells were established by stepwise exposure to osimertinib and simultaneously harbored *EGFR* E762K mutation. In addition, functional studies of *EGFR* E762K mutation confirmed that this mutation acts as a resistant mechanism of EGFR TKIs.

Conclusions: Osimertinib is active against *EGFR* exon 20 insertion-mutant NSCLC and flexibly binds within drug-binding pockets.

Keywords: non-small cell lung cancer, EGFR, exon 20 insertion, resistance, osimertinib

***Student number**: 2015-22059*

CONTENTS

LIST OF TABLES AND FIGURES

Introduction

Lung cancer, especially non-small cell lung cancer (NSCLC), is the top-ranked death related disease over the world [1]. Among NSCLC in Korea, the frequencies of most occurring driver oncogenes; epidermal growth factor receptor (*EGFR*), anaplastic lymphoma kinase (ALK), oncogene in Kirsten RAt Sarcoma virus (KRAS), and Neuroblastoma RAS viral oncogene homolog (NRAS) are about 60.5%, 4.0%, 12.0% and 1.5%, respectively [2-4].

EGFR is an ErbB family member including human epidermal growth factor receptor (HER) 2 - 4, and located chromosome 7p 11.2 and encodes 1,210 amino acids.

Classically, exon 19 in-frame amino acidic deletions that is from E746 to A750, and Leucine (L) to Arginine (R) substitutive point mutation on amino acid 858 in exon 21 represent more than 80% within *EGFR* mutations. The 1st-generation Food and Drug Administration (FDA) approved EGFR tyrosine kinase inhibitors (TKIs), gefitinib or erlotinib, prolonged survival in NSCLC patients with those *EGFR* mutations [5]. However, about 50% of those 1st-generation EGFR TKIs usage induces acquired resistance such as a gate keeper T790M substitutive mutation. To overcome T790M mutation, the 3rd-generation EGFR TKIs (including lazertinib, nazartinib, olmutinib, osimertinib, and rociletinib) were developed and those TKIs were effective against T790M mutation, especially osimertinib that showed the most efficacy with blood brain barrier (BBB) penetrating and was recently approved by FDA.

Occurrence of classic *EGFR* mutations were followed by *EGFR* exon 20 insertion mutations as 4 to 10% of *EGFR* mutant lung cancers [6]. *EGFR* exon 20 insertions arise between amino acid from 761 to 775, αC-β4 loop of EGFR. *EGFR* exon 20 insertion mutations are unusually diverse as not only occurring sites but also inserted amino acid types. Thus, about a hundred various insertion subtypes are. Depending on what and where amino acidic insertion(s) occurred, those have different drug efficacies. Previous preclinical and clinical studies revealed that gefitinib and erlotinib have no inhibitory effect and the 2nd-generation EGFR TKI, afatinib had short medial progression free survival (PFS) as 2.7 months (LUX-Lung) [7]. Another 2nd-generation EGFR TKI, poziotinib showed 64% of objective response rate (ORR) against *EGFR* exon 20 insertion mutant lung cancer patients [8]. However, the most recently clinical data showed 5.5 months of progression free survival (PFS) with dose reduction for 60% of poziotinib-treated patients [9]. Most subtypes of *EGFR* exon 20 insertion mutations are resistant to the 1st- and the 2nd-generation EGFR TKIs, however, a subtype A763insFQEA is susceptible to those TKIs. Even though those EGFR TKIs are less effective against *EGFR* exon 20 insertion mutations, efficacy of the 3rd-generation EGFR TKIs are contentious.

Here, we developed seven kinds of *EGFR* exon 20 insertion mutant Ba/F3 models, A763insFQEA, V769insSVD, D770insSVD, D770insNPG, P772insPR, H773insH, H773insNPH, and *EGFR* H773insAH mutant lung cancer patient-derived cell line, SNU-3173. With those mutant models, we performed cell viability assay, immunoblot assay, and N-ethyl -N-nitrosourea (ENU) mutagenesis screening with several EGFR TKIs; erlotinib, gefitinib,

afatinib, dacomitinib, poziotinib, nazartinib, olmutinib, osimertinib, and rociletinib. In addition, we constructed *in silico* homology models to compare structural changes among *EGFR* mutants, and to correlate with *in vitro* data.

Materials and methods

1. Cell lines and reagents

Human embryonic cell line 293T (ATCC CRL-11268), KRAS G12S mutant non-small cell lung cancer (NSCLC) cell line, A549 (ATCC CCL-185) and *EGFR* L858R/T790M mutant cell line, NCI-H1975 (ATCC CRL-5908), were purchased from American Type Culture Collection (ATCC; Manassas, Virginia), *EGFR* E746-A750 deletion mutant cell line, PC9 was kindly provided by Dr. Mayumi Ono (Kyushu University, Fukuoka, Japan). Mouse pro-B-cell line Ba/F3 was purchased from the Deutsche Sammlung von Mikroorganismen und Zellkulturen (DSMZ, Braunschweig, Germany). SNU-3173 cells were derived at diagnosis from a 46-year-old male patient with stage IV NSCLC with *EGFR* H773insAH mutation who failed after one cycle of pemetrexed and cisplatin and subsequently died 3 months after diagnosis (Institutional Review Board [IRB] No. 1102-098-357). Non-small cell lung cancer cell lines, SNU-3173, PC9, A549, and NCI-H1975 were grown in RPMI-1640 medium supplemented with 10% Fetal Bovine Serum (Gibco, Carlsbad, CA), 1% penicillin/streptomycin (Gibco). Ba/F3 cells were grown in RPMI-1640 medium supplemented with 10% Fetal Bovine Serum (Gibco, Carlsbad, CA), 1% penicillin/streptomycin (Gibco), and 2mmol/L of L-glutamine and 4ng/mL of interleukin-3 (Prospec, Ness Ziona, Israel). 293T cell line was grown in DMEM medium supplemented with 10% Fetal Bovine Serum (Gibco), and 2mmol/L of L-glutamine. Gefitinib (Iressa), erlotinib (Tarceva), afatinib (Gilotrif), dacomitinib (Vizimpro), poziotinib (HM781-

36B), lazertinib (YH25448), nazatinib (EGF816), olmutinib (HM61713, Olita), osimertinib (AZD9291, Tagrisso), and rociletinib (CO-1686) were purchased from Selleck chemicals (Boston, MA).

2. Site-directed mutagenesis and construction of retroviral vector-transduced Ba/F3 cells

EGFR exon 20 insertion variant cDNAs produced by site-directed mutagenesis (Agilent Technologies, La Jolla, CA) on the *EGFR* wild-type retroviral vector pBabe-puro, additionally pBabe *EGFR* insertion H (H773insH) and *EGFR* D770insNPG (D770_N771insNPG) that was a gift from Matthew Meyerson40 (Addgene plasmid #11011, #32067, and #11016 respectively) with designed mutant specific primers (Table 1) [10]. Mutant cDNAs were inserted into TOPO-TA cloning vector (Invitrogen, CA, USA) and then analyzed by electropherogram, confirmed with The Basic Local Alignment and Search Tool (BLAST, NCBI). Each *EGFR* exon 20 insertion variants were transfected into Ba/F3 cells. Retroviral-transduced Ba/F3 cells are selected by puromycin treatment and subsequently cultured in IL-3 absent medium for 4 weeks.

3. Cell proliferation assays

Constructed *EGFR* exon 20 insertion variant harboring Ba/F3 cells and EGFR mutant lung cancer cells; SNU-3173, PC9, NCI-H1975, and A549 were cultured as 3 x 10^3/well in 96-well plates with RPMI1640 medium with diluted EGFR TKIs for 72 hours. EGFR TKIs; gefitinib, erlotinib, afatinib, dacomitinib,

poziotinib, lazertinib, nazartinib, olmutinib, osimertinib, and rociletinib were diluted by a factor of 10. Cell proliferation analyzed using CellTiter Glo-Luminescent cell viability assay (Promega, Madison, WI, USA) and the luminescent signal was measured by GloMax® Navigator Microplate Luminometer (Promega). Concentrations that inhibits 50% (IC_{50}) values and graphs were determined using Sigmaplot 12.0 software (Systat Software Inc., San Jose, California) and GraphPad Prism 6 software (GraphPad Software, San Diego, California). These experiments were repeated three times independently.

4. Immunoblot assay

Cells were plated on the 6-well plates and treated with EGFR TKIs with 100 nmol/L and 1 μmol/L for 4 hours. Subsequently, cell lysis proceeded with diluted 10X Cell lysis buffer (Cell Signaling Technology, Danvers, USA), Phenylmethylsulfonyl fluoride (Sigma, USA), PhosSTOP (ROCHE, Swiss), and Proteinase Inhibitor Cocktail (Merck, USA) and quantified with protein assay dye reagent concentrate (Bio-Rad, USA). Prepared samples were separated through NuPAGE Bis-Tris Gels (Invitrogen, USA), transferred to Polyvinylidene difluoride (PVDF) membranes (Bio-Rad, USA), and detected with ECL Prime Western Blotting Detection Reagent (GE healthcare, UK). To detect EGFR signaling pathway, total-EGFR (#4267S), phosphor-EGFR (#3777S), total-AKT (#4685), phosphor-AKT (#4060S), total-ERK 42/44 (#9102), phosphor-ERK (#9106), and GAPDH (#5174) were used and

purchased from Cell Signaling Technology (Danvers, MA). Image analysis was carried out with ImageQuant LAS4000mini (GE healthcare, UK).

5. Colony-forming assay

SNU-3173 cells were plated at 1 x 10^3/well in 12-well plates with RPMI-1640 media and incubated overnight. After cells adhered, osimertinib was added at 50, 100, and 500 nM concentration within 1 mL of RPMI1640 culture media. Drugs and media were changed every 3 days for 3 weeks. Cells were washed twice with Dulbecco's Phosphate-Buffered Saline (Gibco), fixed for 30 minutes in absolute ethanol at room temperature, and washed with distilled water. Cells were stained for 10 minutes with 0.1% Brilliant Blue (Sigma-Aldrich) and washed three times with distilled water. Stained cells were captured and counted with the EVOS Cell Imaging System (Thermo Fisher, Waltham, Massachusetts).

6. Polymerase chain reaction (PCR) and quantitative real time-PCR (qPCR)

Genomic DNA was isolated from the SNU-3173 patient-derived cell pellet and *EGFR* exon 20 insertion mutant Ba/F3 cell pellets; A763insFQEA, V769insASV, D770insSVD, P772insPR, H773insH, and H773insNPH, using an ALL-prep DNA/RNA micro kit (Quiagen, USA). *EGFR* exons were amplified with designed primers (Table 2) and High Fidelity plus PCR system (Roche, USA). Cycling conditions were 95℃ for 10 minutes, followed by 35

cycles at 95℃ for 20 seconds, 58℃ for 30 seconds, and 72℃ for 30 seconds. Subsequently, sequenced by direct sequencing with specific primers.

7. Computational atomistic modeling and osimertinib docking simulation

EGFR wild-type (PDB ID: 4ZAU), L858R/T790M (PDB ID: 4RJ5) and D770insNPG (PDB ID: 4LRM) protein crystallized models were developed and able to use through Protein data base (http://www.rcsb.org/pdb/), but the other EGFR exon 20 insertion mutant protein (A763insFQEA, V769insASV, D770insSVD, P772insPR, H773insH, H773insNPH, and H773insAH) predictive models were constructed by SWISS-MODEL [11]. Docking simulation and delta G value calculation of these atomistic models with osimertinib was proceeded by SwissDock [12]. Constructed models and docking simulations were visualized and analyzed with UCSF Chimera [13].

8. N-Ethyl-N-nitrosourea (ENU) mutagenesis screening

EGFR exon 20 insertion mutant harboring Ba/F3 cells were plated as the number of $5x10^6$ cells/mL and exposed to 50 μg/mL of N-Ethyl-N-nitrosourea (ENU) for 24 hours. After exposing, *EGFR* exon 20 mutant harboring Ba/F3 cells were washed with RPMI1640 three times and cultured to grow exponentially. Plating ENU exposed grown cells to 96-well plates as $1x10^6$ cells/well and add compounds as concentration as 500 nM to 1μM. Inspection with light microscope as 2 to 4 day intervals and change the media with compounds. Extract DNA of well-growing cells, amplify DNA region between

EGFR exon 18 to 25 through PCR amplification, and analyzed through directed-sequencing.

primer name		sequence (5' to 3')
A763_Y764insFQEA	F	AATCCTCGATGAAGCCTTCCAGGAAGCCTACGTGATGGCCAGCG
	R	CGCTGGCCATCACGTAGGCTTCCTGGAAGGCTTCATCGAGGATT
D770_N771insSVD	F	CGTGATGGCCAGCGTGGACAGCGTGGACAACCCCC
	R	GGCACACGTGGGGGTTGTCCACGCTGTCCACGC
V769_D770insASV	F	GATGGCCAGCGTGGCCAGCGTGGACAACCCCCACGTG
	R	CACGTGGGGGTTGTCCACGCTGGCCACGCTGGCCATC
H773_V774insNPH	F	GGACAACCCCCACAACCCCCACGTGTGCCGCCTGC
	R	GCAGGCGGCACACGTGGGGGTTGTGGGGGTTGTCC
P772_H773insPR	F	GTGGACAACCCCCCCCGCCACGTGTGCCGC
	R	GCGGCACACGTGGCGGGGGGGGTTGTCCAC

Table 1. Site-directed mutagenesis primers.

primer name		sequence (5' to 3')
EGFR exon 18	F	TCCAAATGAGCTGGCAAGTG
	R	TCCCAAACACTCAGTGAAACAAA
EGFR exon 19	F	CCCAGTGTCCCTCACCTTC
	R	GCAGGGTCTAGAGCAGAGCA
EGFR exon 20	F	CATTCATGCGTCTTCACCTG
	R	CATATCCCCATGGCAAACTC
EGFR exon 21	F	GCTCAGAGCCTGGCATGAA
	R	CATCCTCCCCTGCATGTGT

Table 2. Primers for PCR amplification of *EGFR* exons.

Results

Construction of *EGFR* exon 20 insertion mutant models

Various *EGFR* exon 20 insertion mutations were listed up with Catalogue Of Somatic Mutation In Cancer (COSMIC) data base [14]. *EGFR* exon 20 insertion mutations occurred in αC-helix (amino acids from 761 to 766) and following loop (amino acids from 767 to 775) within exon 20, and interestingly, more than 90% of *EGFR* exon 20 insertion mutations rise in the following loop. Especially, amino acids after 769, 770, and 773 are the most insertion mutation incident sites as 55.4% of total exon 20 insertions (Table 3). Seven kinds of *EGFR* exon 20 insertion subtypes were selected including A763insFQEA, A769insASV, D770insSVD, D770insNPG, P772insPR, H773insH, and H773insNPH that are frequently occurring more than half of *EGFR* exon 20 insertion subtypes for experimental model constructions (Figure 1 and Table 4). Cloned *EGFR* exon 20 insertion mutant plasmids were transfected into Ba/F3 mice pro-B cells that can grow and expand with IL-3 dependently. All *EGFR* exon 20 insertion mutant Ba/F3 cells grew well with IL-3 independent condition after selections (Figure 2), and each mutation transfected into Ba/F3 cells were confirmed with direct sequencing (Figure 3).

	insertion after	counts	%
αC-helix	761	4	1.0%
	763	16	3.9%
	764	2	0.5%
	765	1	0.2%
The following loop	767	34	8.3%
	768	34	8.3%
	769	75	18.2%
	770	79	19.2%
	771	48	11.7%
	772	37	9.0%
	773	74	18.0%
	774	7	1.7%
Total		411	100%

Table 3. The ratios of *EGFR* exon 20 insertion occurring positions.

The following amino acidic positions that insertion mutants rise from 761 to 774. The incidences divided by structural characteristic within αC-helix (amino acids from 761 to 766) and following loop (amino acids from 767 to 775) are 5.6% and 94.4%, respectively. Data obtained from COSMIC data base.

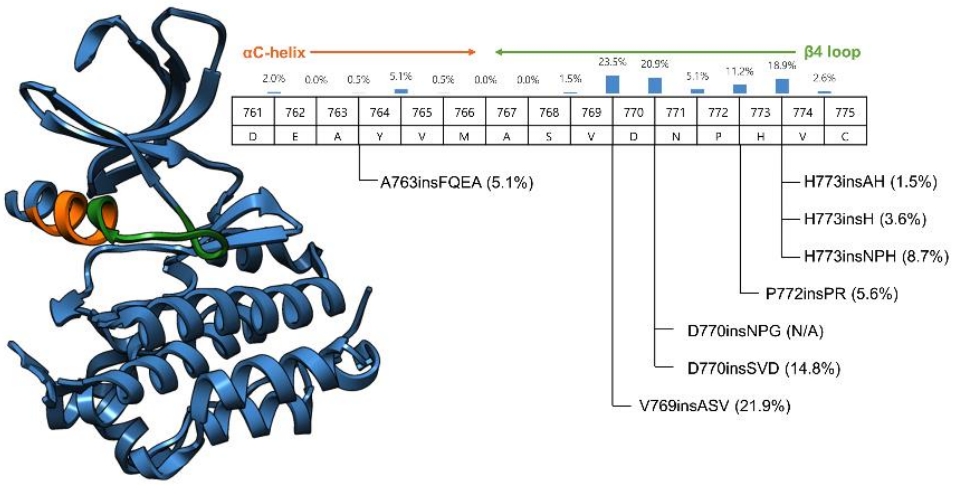

Figure 1. The structural model of EGFR and incidence of selected *EGFR* exon 20 insertion mutations.

EGFR exon 20 insertion mutations occurs amino acids from 761 to 775 that form C-helix and C-helix following loop. The scheme of helix and loop structures are colored with orange and green, respectively. Described mutant subtypes were selected and used in this study.

#	Mutations	Abbr	Sequence																				
			761	**762**	**763**	**764**	**765**	**766**	**767**	**768**	**769**	**770**	**771**	**772**	**773**	**774**	**775**	**776**	**777**				
-	Wild-type	WT	GAT	GAA	GCC	TAC	GTG	ATG	GCC	AGC	GTG	GAC	AAC	CCC	CAC	GTG	TGC	CGC	CTG				
			D	E	A	Y	V	M	A	S	V	D	N	P	H	V	C	R	L				
1	A763_Y764insFQEA	FQEA	GAT	GAA	GCC	TTC	CAG	GAA	GCC	TAC	GTG	ATG	GCC	AGC	GTG	GAC	AAC	CCC	CAC	GTG	TGC	CGC	CTG
			D	E	A	**F**	**Q**	**E**	**A**	Y	V	M	A	S	V	D	N	P	H	V	C	R	L
2	V769_D770insASV	ASV	GAT	GAA	GCC	TAC	GTG	ATG	GCC	AGC	GTG	GCT	TCT	GTA	GAC	AAC	CCC	CAC	GTG	TGC	CGC	CTG	
			D	E	A	Y	V	M	A	S	V	**A**	**S**	**V**	D	N	P	H	V	C	R	L	
3	D770_N771insNPG	NPG	GAT	GAA	GCC	TAC	GTG	ATG	GCC	AGC	GTG	GAC	AAC	CCC	GGC	AAC	CCC	CAC	GTG	TGC	CGC	CTG	
			D	E	A	Y	V	M	A	S	V	D	**N**	**P**	**G**	N	P	H	V	C	R	L	
4	D770_N771insSVD	SVD	GAT	GAA	GCC	TAC	GTG	ATG	GCC	AGC	GTG	GAC	AGC	GTG	GAC	AAC	CCC	CAC	GTG	TGC	CGC	CTG	
			D	E	A	Y	V	M	A	S	V	D	**S**	**V**	**D**	N	P	H	V	C	R	L	
5	P772_H773insPR	PR	GAT	GAA	GCC	TAC	GTG	ATG	GCC	AGC	GTG	GAC	AAC	CCC	CCC	CGC	CAC	GTG	TGC	CGC	CTG		
			D	E	A	Y	V	M	A	S	V	D	N	P	**P**	**R**	H	V	C	R	L		
6	H773_V774insAH	AH	GAT	GAA	GCC	TAC	GTG	ATG	GCC	AGC	GTG	GAC	AAC	CCC	CAC	GCC	CAC	GTG	TGC	CGC	CTG		
			D	E	A	Y	V	M	A	S	V	D	N	P	H	**A**	**H**	V	C	R	L		
7	H773_V774insH	H	GAT	GAA	GCC	TAC	GTG	ATG	GCC	AGC	GTG	GAC	AAC	CCC	CAC	CAT	GTG	TGC	CGC	CTG			
			D	E	A	Y	V	M	A	S	V	D	N	P	H	**H**	V	C	R	L			
8	H773_V774insNPH	NPH	GAT	GAA	GCC	TAC	GTG	ATG	GCC	AGC	GTG	GAC	AAC	CCC	CAC	AAC	CCC	CAC	GTG	TGC	CGC	CTG	
			D	E	A	Y	V	M	A	S	V	D	N	P	H	**N**	**P**	**H**	V	C	R	L	

Table 4. Nucleobase and amino acid Sequences of selected *EGFR* exon 20 insertion mutant models.

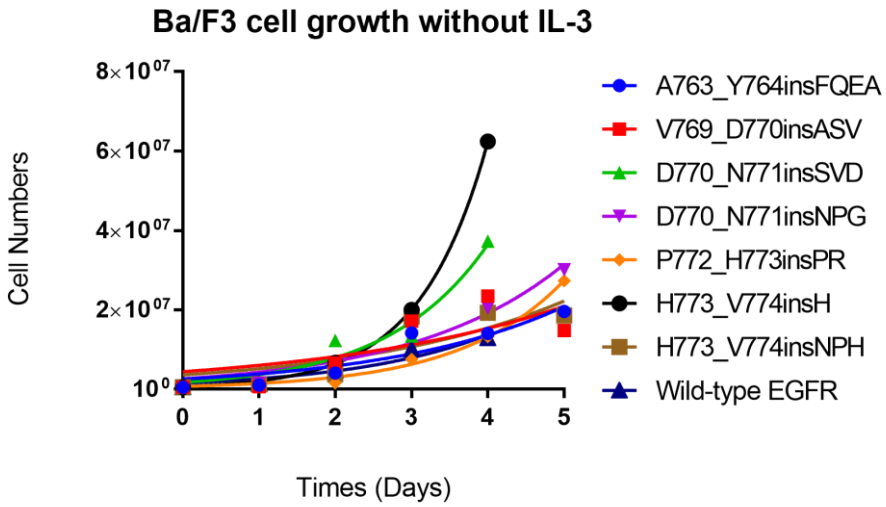

Figure 2. Exponential growth of Ba/F3 cells with *EGFR* exon 20 insertion mutations.

All Ba/F3 cells were selected by dose escalating of puromycin and subsequent IL-3 exception. *EGFR* wild-type Ba/F3 cells were cultured with 30 ng/mL of EGF ligand and other *EGFR* exon 20 insertion mutant Ba/F3 cells grew with oncogenicity of *EGFR* mutations.

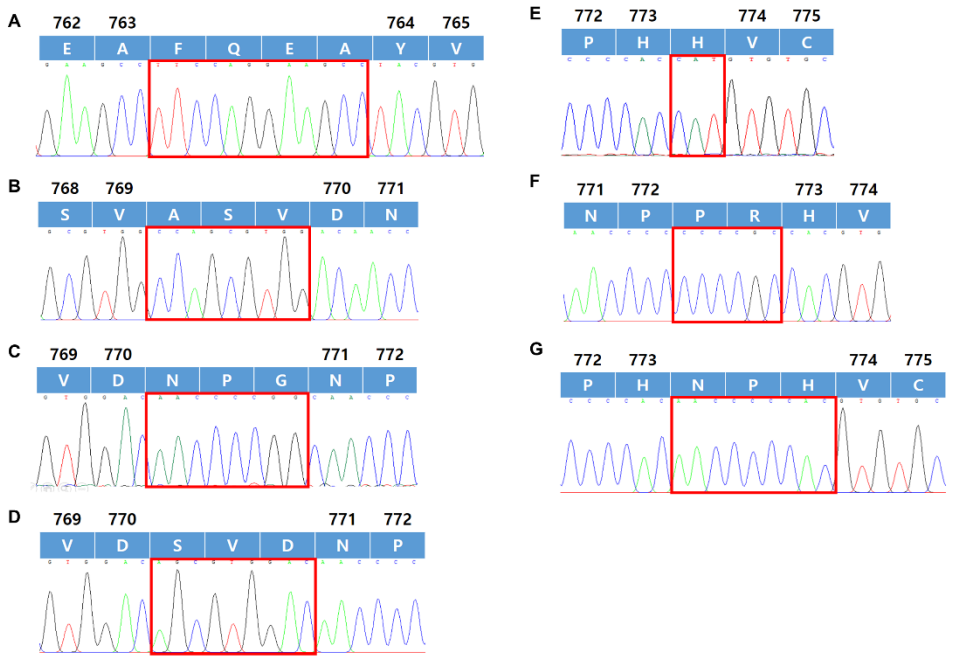

Figure 3. Direct sequencing results of insertion region in *EGFR* exon 20.

DNA extracted from *EGFR* exon 20 insertion mutant Ba/F3 cells and analyzed by direct sequencing. (A) A763insFQEA, (B) V769insASV, (C) D770insNPG, (D) D770insSVD, (E) H773insH, (F) P772insPR, and (G) H773insNPH were identified.

Efficacies of EGFR TKIs against *EGFR* exon 20 insertion mutant Ba/F3 cells

Immunoblot and cell viability assays were performed with constructed *EGFR* exon 20 insertion mutant Ba/F3 cells. The 1st-, 2nd-, and 3rd-generation EGFR TKIs; gefitinib, erlotinib, afatinib, dacomitinib, rociletinib, olmutinib, osimertinib, and nazartinib. Through cell viability assay, we confirmed the trend of EGFR TKIs efficacies against *EGFR* exon 20 insertion mutants. As previously reported [15], inner αC-helix insertion mutation, A763insFQEA Ba/F3 cells showed sensitivity to the 1st- and 2nd-generation EGFR TKIs (0.002 nM to 33.3 nM), on the other hand, 3rd-generation EGFR TKIs were less sensitive (824. nM to 262.9 nM). Except A763insFQEA, the other insertion mutations occur within αC-helix following loop mostly showed resistance to the 1st-generation EGFR TKIs (948.7 nM to 5,391 nM). However, the 2nd- and 3rd-generation EGFR TKIs showed exceptional efficacies compared to gefitinib and erlotinib (Figure 4).

The inhibitory effects of EGFR TKIs were validated through immunoblot assay (Figure 5). As shown in cell viability assay, gefitinib and erlotinib showed phospho-EGFR inhibitory effects only against A763insFQEA mutants (Figure 5B). The inhibited expressions of phospho-EGFR were dose-dependent manner as similar in the results of cell viability assay. Remarkably, the 3rd-generation EGFR TKI, osimertinib downregulated phospho-EGFR in all *EGFR* exon 20 insertion mutant cells, especially osimertinib showed the better efficacy against H773insH than the 2nd-generation EGFR TKIs.

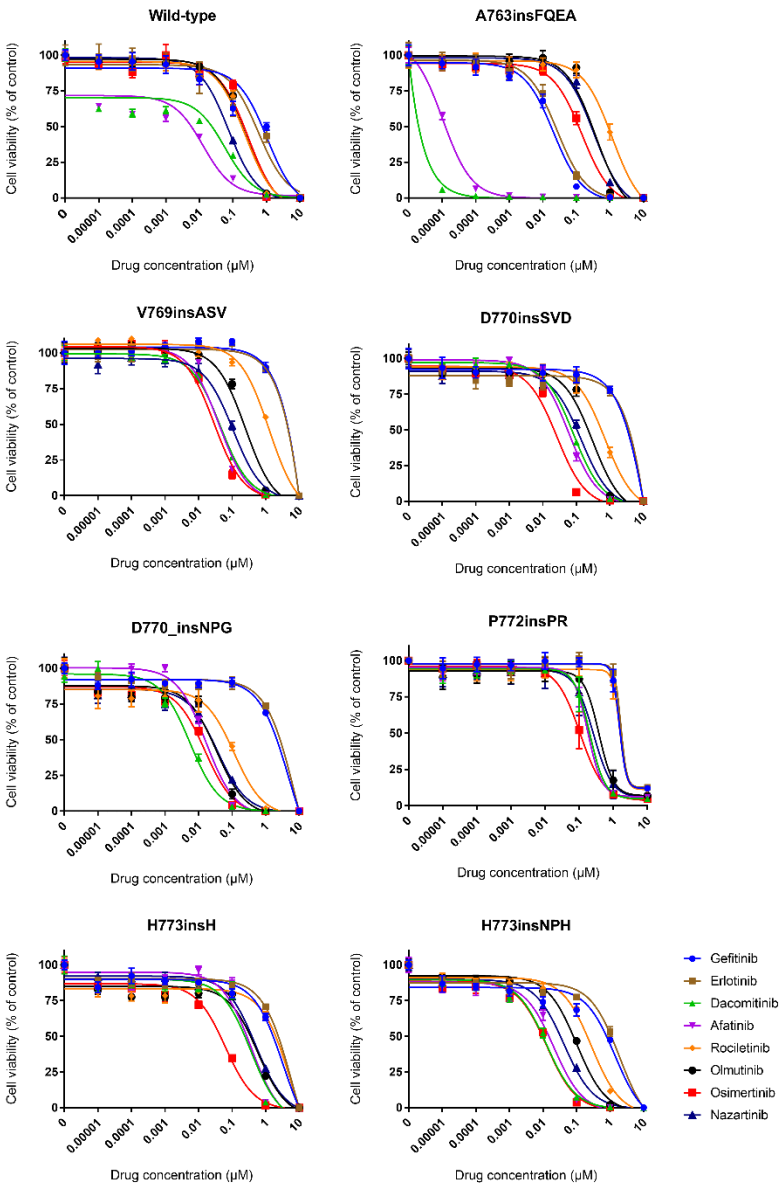

Figure 4. Cell viability assay of *EGFR* exon 20 insertion mutant Ba/F3 cells.

All cells were exposed to EGFR TKIs for 72 hours. These experiments were repeated three times independently, and graphs represent mean values with S.D.

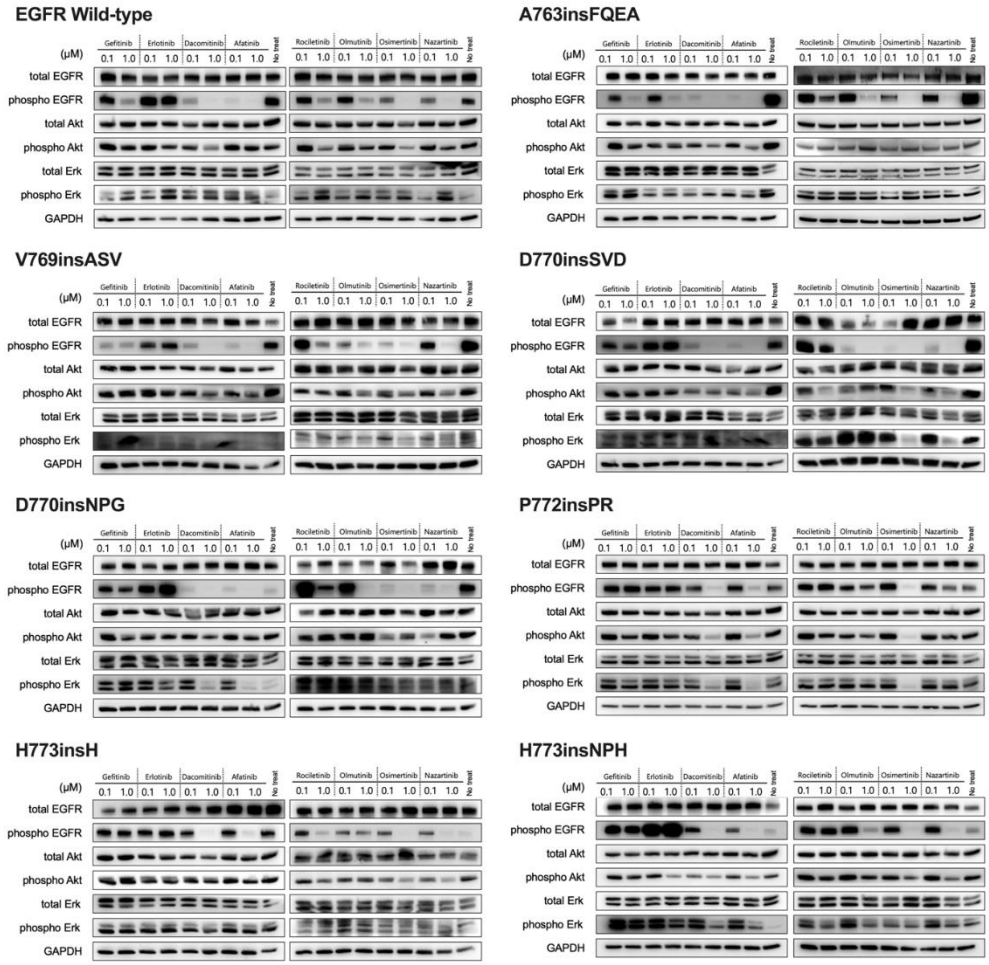

Figure 5. Immunoblot assay of *EGFR* mutant Ba/F3 cells.

All cells were treated with EGFR TKIs as concentrations of 100 nM and 1 μM for 4 hours. The housekeeping gene GAPDH was used as a loading control.

EGFR TKIs susceptibility of patient-derived cell line, SNU-3173

A stage IV lung adenocarcinoma patient took several cycles of chemotherapies (detailed in Material and Methods), but died after 3 months for fast growth of tumors (Figure 6). SNU-3173, a cell line extracted from this patient, was established and detected H773insAH mutation through direct sequencing of *EGFR* exon 20 cDNA cloned into *E.coli* colony (Figure 7A). As performed Ba/F3 cells above, SNU-3173 cells were treated EGFR TKIs for cell viability assay and immunoblot assay. Similarly, cell viability assay of SNU-3173 (Figure 7B) showed resistance to gefitinib and erlotinib (1050.5 nM to 4535.5 nM), and sensitive efficacies of afatinib and dacomitinib (13.7 nM to 16.7 nM). The efficacies of the 2nd-generation EGFR TKIs were followed by osimertinib (62.7 nM). Immunoblot assay of SNU-3173 also showed consisted with the results of Ba/F3 cells, down signaling pathway phospho-Erk also regulated by afatinib and dacomitinib as well as osimertinib, but not affected to Akt (Figure 7C).

To confirm the anti-cancer effect of osimertinib, 2D colony forming assay was performed. Compared to non-treat control, 50 nM of osimertinib inhibited colony formation of SNU-3173 cells by about 70% (Figure 8).

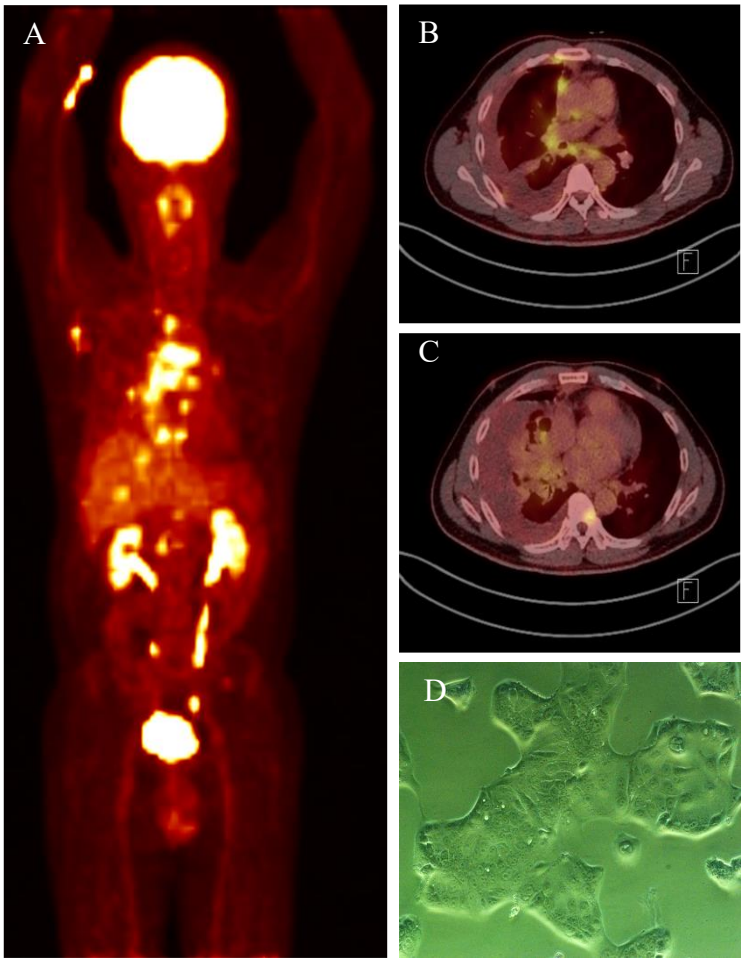

Figure 6. The tumor of a patient (46-year old male) with *EGFR* exon 20 insertion mutant lung adenocarcinoma and his patient-derived cell lines (SNU-3173).

(A-C) At diagnosis, he experienced tumors progression after failure to one cycle of pemetrexed and cisplatin. (D) SNU-3173 cells were obtained from the patient pleural effusion.

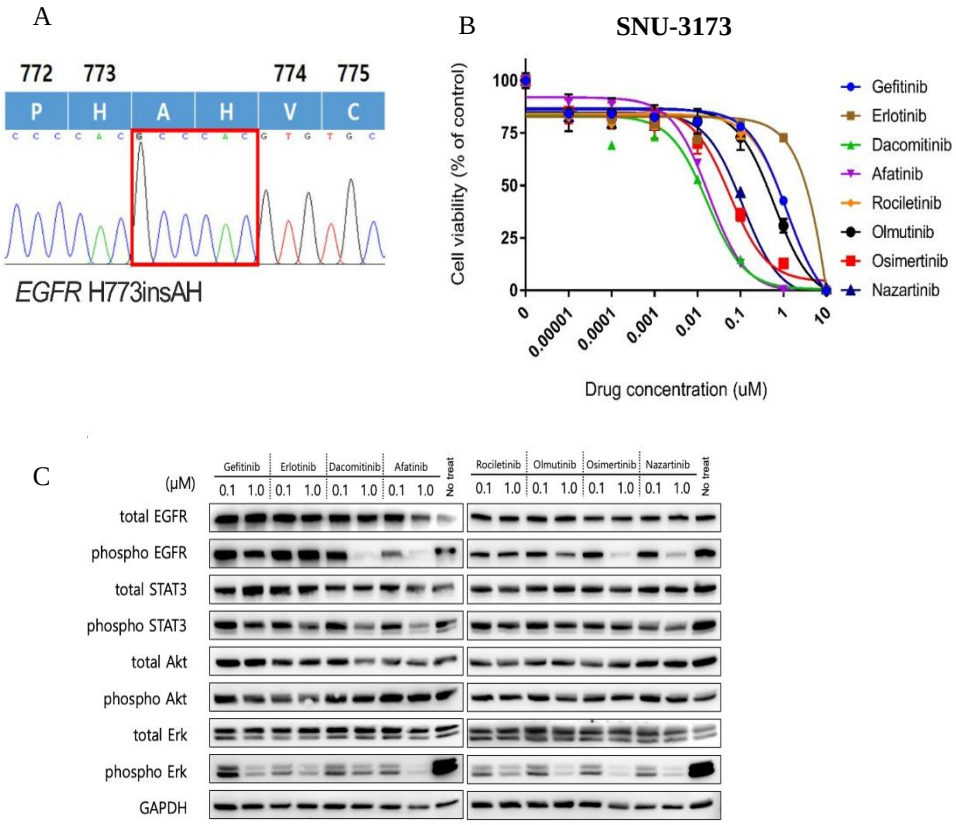

Figure 7. Characterizations of SNU-3173 cells.

(A) direct sequencing of a clonal cDNA of SNU-3173. (B) Cell viability assay of EGFR exon 20 insertion mutant Ba/F3 cells. All cells were exposed to EGFR TKIs for 72 hours. These experiments were repeated three times independently, and graphs represent mean values with S.D. (C) Immunoblot assay of SNU-3173 cells. All cells were treated with 100 nM or 1 μM EGFR TKIs for 4 hours. The housekeeping gene GAPDH was used as a loading control.

A

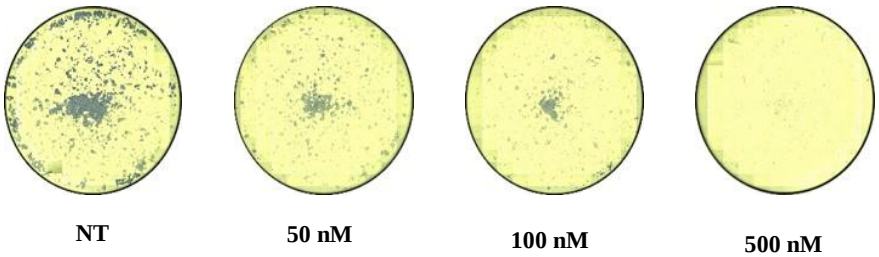

NT 50 nM 100 nM 500 nM

B

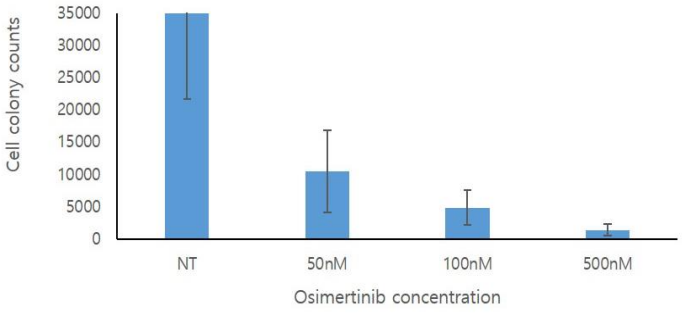

Figure 8. Colony forming assay of SNU-3173 cells.

(A) SNU-3173 cells were treated with osimertinib for 3 weeks with several concentrations and then stained. Cell images were captured and analyzed with the EVOS Cell Imaging System. (B) Graphs of counted colonies. Colonies counted using Celleste Image Analysis Software (Invitrogen by Thermo Fisher Scientific). These experiments were repeated three times independently, and graphs represent mean values with S.D.

Prediction of osimertinib toxicities

With the results of cell viability assay (Table 5), we could compare the EGFR TKI sensitivities between *EGFR* wild-type and exon 20 insertion mutants. Comparing IC_{50} values as log10 ratio in *EGFR* mutant versus wild-type cells, the values simplified the susceptibilities of EGFR TKIs. Although afatinib and dacomitinib showed the most sensitive toxicities against *EGFR* exon 20 insertion mutants, those compounds also sensitive to *EGFR* wild-type. However, osimertinib that is similarly sensitive against *EGFR* exon 20 insertion mutants compared to afatinib and dacomitinib showed sparing effect to *EGFR* wild-type cells, and it is shown as the under zero in log-ratio values (Figure 9).

IC50 (nM) / ± S.D.	WT (+EGF 30ng/mL)	FQEA	ASV	SVD	NPG	PR	H	NPH	SNU-3173	PC9	H1975	A549
Gefitinib	1127 / 90	21.7 / 4	4870.1 /288.5	3479.3 / 790.9	2422 / 267.3	3611.4 / 1178.1	1980.1 / 288.7	948.7 / 138.5	1050.4 / 66.8	10.9	7212.2	3716
Erlotinib	1333.1 / 173.3	33.3 / 5.1	5050.7 / 520.5	5179.7 / 393.3	3240.1 / 289.7	5391 / 115.1	2858.7 / 337.2	1391 / 236.6	4535.5 / 321	14.9	5409.3	2950.2
Dacomitinib	39 / 4.4	0.002 / 0.00019	55.4 / 2.1	85.9 / 3.8	7.5 / 0.7	161.8 / 18.7	320.2 / 34.8	10.8 / 1.8	13.7 / 1.6	0.0043	83.5	1482.3
Afatinib	7.3 / 0.4	0.013 / 0.00092	54.1 / 3.3	63.8 / 6.7	16.7 / 2.1	200 / 10.4	352.5 / 22.7	19.5 / 3	16.7 / 2.2	0.0232	96	1158.4
Rociletinib	262.9 / 25.7	1022.1 / 172.8	1324.9 / 66.7	731.8 / 61.1	96.7 / 12.9	3034.6 / 689.8	2309.4 / 401.4	288 / 25	1202.5 / 158.2	62.8	24.2	3123
Olmutinib	236.2 / 16.4	351.8 / 20.2	262.3 / 20.8	287.7 / 29.5	30.4 / 3.9	314.3 / 27.6	497.6 / 50.5	97.3 / 2.7	626.7 / 31.6	8.5	3.3	5062.3
Osimertinib	259.2 / 22.7	131.6 / 19	41 / 4.0	28.1 / 2.9	14.7 / 2.2	22.4 / 3.9	65.7 / 4.5	11.4 / 1.3	62.7 / 7.3	0.52	1.5	1609.9
Nazartinib	82.4 / 4.9	351.8 / 28.6	108.2 / 6.9	128.5 / 17	36.3 / 4.1	147.7 / 13.4	509.9 / 58.4	49.6 / 1.8	139.7 / 13.6	4.2	12.8	2782

Table 5. IC_{50} values of *EGFR*-mutant cells.

IC_{50} values were obtained from cell viability assays. Human lung cancer cell lines, PC9 (exon 19 in-frame deletion, E746-A750del), NCI-H1975 (EGFR L858R/T790M), and A549 (KRAS G12S) were used as controls for EGFR TKIs. *EGFR* exon 20 insertion-mutant Ba/F3 cells, A763insFQEA, V769insASV, D770insSVD, D770insNPG, P772insPR, H773insH, and H773insNPH are abbreviated as FQEA, ASV, SVD, NPG, PR, H, and NPH, respectively.

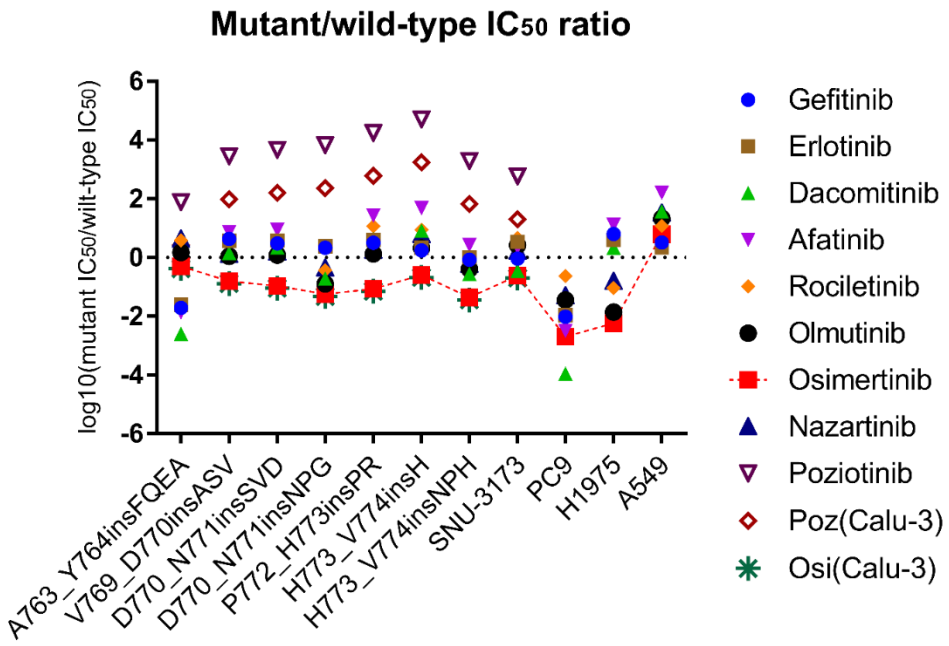

Figure 9. *EGFR* mutant to wild-type IC_{50} ratios of EGFR TKIs against *EGFR*-mutant cells.

EGFR mutant to wild-type IC_{50} ratios were calculated as concentration that inhibits 50% (IC_{50}) values of *EGFR*-mutant cells divided by those of *EGFR* wild-type cells. The smaller value predicts smaller toxicities associated with sparing of wild-type *EGFR* cells. Individual values were calculated from **Table 5**. PC9, H1975, and A549 cells were used as controls for EGFR TKIs.

Homology modeling of *EGFR* exon 20 insertion mutants

We showed the efficacies of EGFR TKIs against *EGFR* exon 20 insertion mutants above. However, *EGFR* exon 20 insertion mutation has not been well characterized. Thus, we constructed homology models of *EGFR* exon 20 insertion mutants based D770insNPG protein data (PDB ID: 4LRM) and compared structural differences among *EGFR* exon 20 insertion mutant models (Figure 10). As previous study revealed, A763insFQEA mutant make one more helix-turn and this additional turn make the 1st- and 2nd-generation EGFR TKIs bind well within the drug binding pocket (Figure 10B) [15]. Except A763insFQEA, all the other mutations are positioned in αC-helix following loop and resistant to the 1st-generation EGFR TKIs. Compared to A763insFQEA, all the other insertion mutations have shorter insertions as one to three amino acid(s) insertions (Figure 10). Additionally, we compared PDB models between osimertinib-sensitive EGFR L858R/T790M (PDB ID: 4RJ5) and EGFR D770insNPG (PDB ID:4LRM) (Figure 11). Different from EGFR L858R/T790M mutant, D770insNPG mutant twisted the αC-helix following loop and this twist continuously forced the P-loop bent down into drug binding pocket (Figure 12).

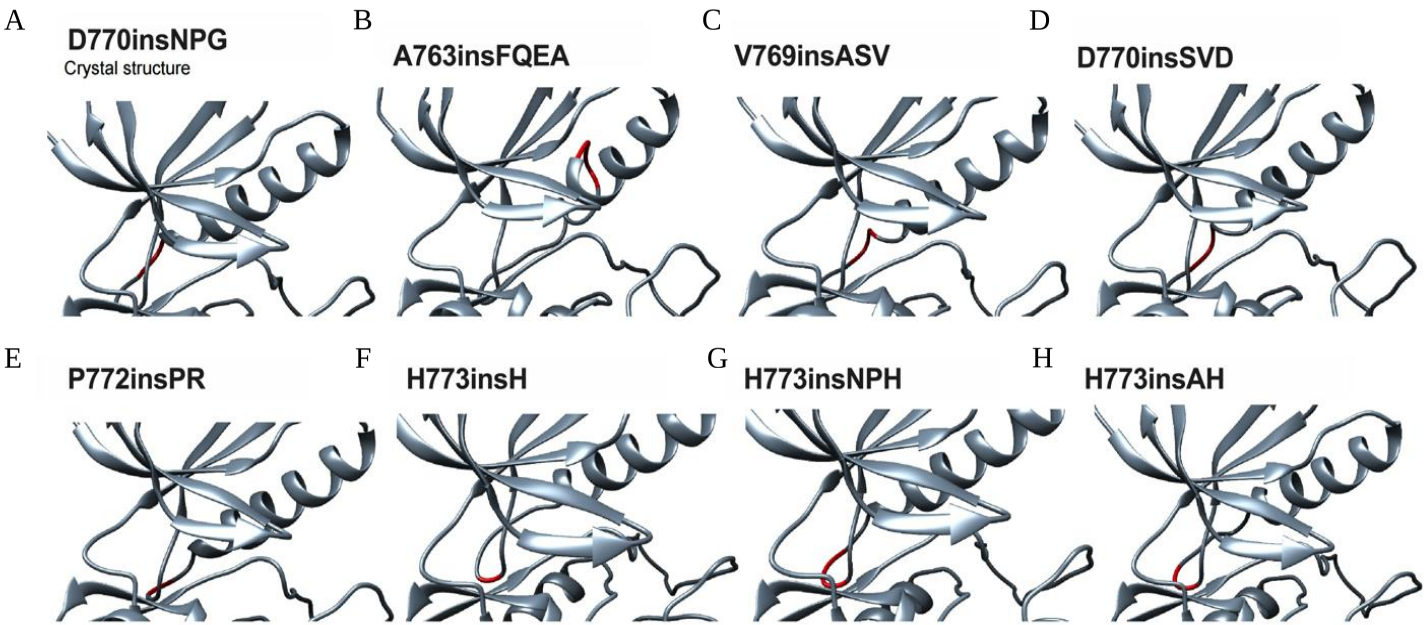

Figure 10. Predictive structural differences between EGFR exon 20 insertion mutants.

D770insNPG (PDB ID: 4LRM) was used as template, and other EGFR exon 20 insertion-mutant homology models were constructed using SWISS-MODEL. Red ribbons indicate inserted amino acids. Structures were handled with UCSF Chimera.

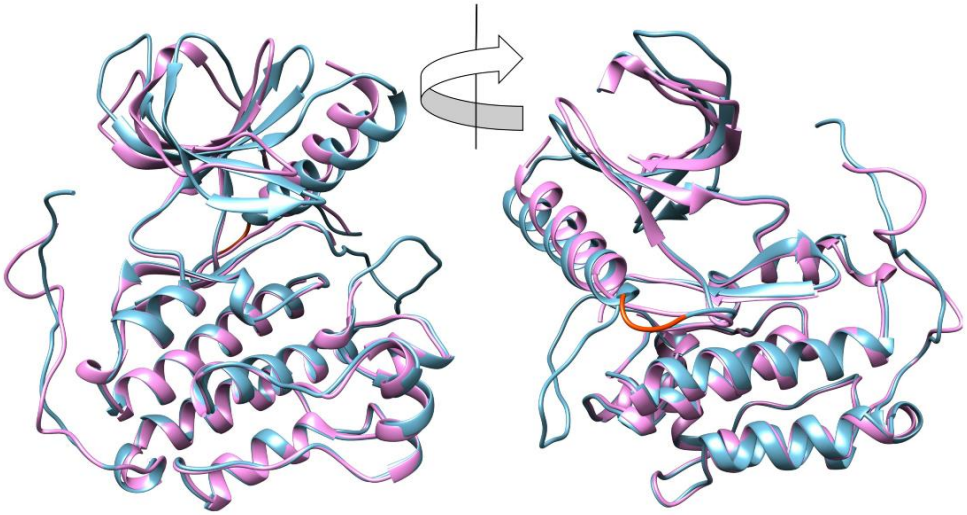

Figure 11. Structural comparisons between mutant EGFR.

EGFR L858R/T790M (PDB ID: 4RJ5, pink) and D770insNPG (PDB ID: 4LRM, light blue) were merged. Structures were turned and showed both the drug-binding side and the Asparagine-Proline-Glycine (NPG) amino acids-inserted side.

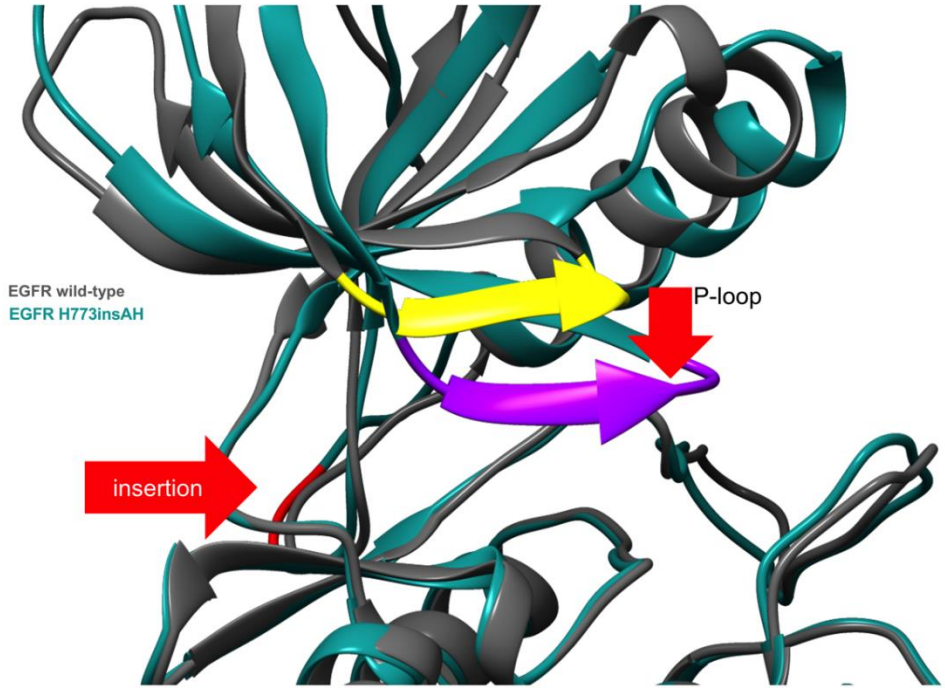

Figure 12. Predictive structural changes between EGFR wild-type and H773insAH.

EGFR wild-type crystal structure (PDB ID: 4ZAU) and the homology model of H773insAH constructed by SWISS-MODEL were merged by UCSF Chimera. Grey ribbons indicate EGFR wild-type, and green ribbons indicate H773_V774insAH. Each phosphate-binding loops (known as nucleotide binding loops) were colored differently as yellow and purple. Red arrows indicate structural changes between EGFR wild-type and H773insAH mutant.

Docking simulations of osimertinib against *EGFR* mutants

After constructing and comparing of *EGFR* exon 20 insertion mutants, we tried to reveal the osimertinib efficacies. Based on computational models, we docked osimertinib on the EGFR mutants (*EGFR* L858R/T790M versus D770insNPG), and osimertinib showed binding appearance similar to each other mutants. Even though P-loop bent condition in *EGFR* D770insNPG, osimertinib could bind flexibly into drug binding pocket (Figure 13). Also we constructed the H773insAH homology model that SNU-3173 has, and simulated docking of osimertinib. We compared the binding appearances and IC_{50} values of osimertinib against between *EGFR* H773insAH and wild-type (Figure 14).

Additionally, to verify correlations between inhibitory effects of osimertinib and structural affinity, we simply compared structural binding affinity (delta G values) and TKI inhibitory effects (IC_{50} values) of L858R/T790M, D770insNPG, and H773insAH, and this result showed somewhat correlations (R^2=0.6406) (Figure 15).

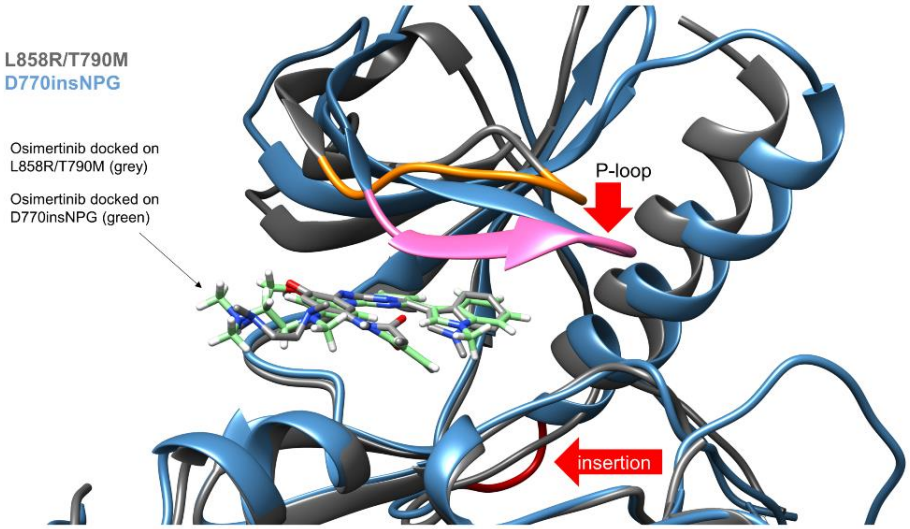

Figure 13. Docking simulations of mutant EGFR.

Previously constructed crystal structures of the EGFR mutants with grey- and partial orange-colored ribbons and blue- and partial pink-colored ribbons indicate EGFR L858R/T790M mutation (PDB ID: 4RJ5) and D770insNPG mutation (PDB ID: 4LRM), respectively. Osimertinib docked on EGFR L858R/T790M and D770insNPG are indicated as grey and green, respectively. Red arrows indicate structural changes between models.

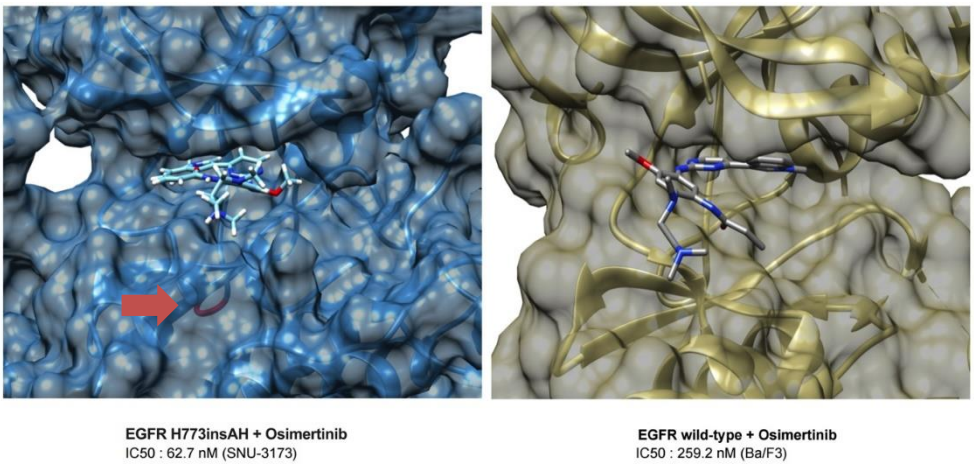

Figure 14. Docking simulation and IC_{50} values of osimertinib on EGFR wild-type and H773insAH.

Osimertinib docked on EGFR wild-type crystal structure (PDB ID: 4ZAU) and EGFR H773insAH homology model compared together with IC_{50} values obtained in the cell viability assay. Red arrow indicates the H773_V774insAH mutation.

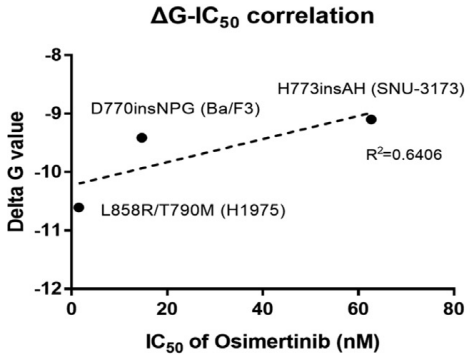

EGFR mutation	Osimertinib IC_{50} (nM)	ΔG
L858R/T790M (H1975)	1.5	-10.606467
D770insNPG (Ba/F3)	14.7	-9.411129
H773insAH (SNU-3173)	62.7	-9.098006

Figure 15. Correlation of IC_{50} values and docking simulation for EGFR L858R/T790M, D770inNPG, and H773insAH.

Delta G values were calculated using Swiss-Dock and the graph and coefficient of determination R^2 determined using Graphpad 6.0.

Spectrum of osimertinib resistant mutations for *EGFR* exon 20 insertions

Even though osimertinib is potent to inhibition of *EGFR* exon 20 insertion mutants, acquired resistance is unavoidable. Thus, ENU mutagenesis screening was performed to identify additional acquired *EGFR* mutations after using osimertinib against *EGFR* exon 20 insertion mutations. *EGFR* D770insSVD, H773insH, and H773insNPH harboring Ba/F3 cells were exposed to ENU for 24 hours and then selected with osimertinib. E762K mutation was the most frequently occurred (Figure 16A), and various mutations that are located in the ATP-binding sites in exon 20 including previously identified the 3rd-generation EGFR TKIs resistant mechanisms; L792I/S, P794S, and G796D detected (Figure 16C and D) [16-22]. Even though we screened osimertinib resistant *EGFR* mechanisms, well-identified resistant mutation, C797S was not found (Figure 17 and Table 6). However, we developed *EGFR* C797S positive exon 20 insertion Ba/F3 models, and performed cell viability assay to confirm the osimertinib resistance (Figure 18).

Furthermore, we developed an osimertinib-resistant SNU-3173OR cell, and *EGFR* E762K was simultaneously identified that was found in ENU screening (Figure 19A). This SNU-3173OR cells were also resistant to osimertinib (Figure 19B). *EGFR* A769insASV/E762K Ba/F3 cells were developed and were performed cell viability assay, and those cells showed resistance to osimertinib as well as poziotinib (Figure 19C). To confirm the resistance mechanism of E762K mutation, we developed *EGFR* exon 20 insertion/E762K transient expressing HEK 293T cells, and verified with immunoblot assay. V769insASV/E762K and H773insH/E762K mutant *EGFR* expressing 293T

cells were treated with gefitinib, afatinib, poziotinib, and osimertinib. However, poziotinib alone showed marginal inhibition of EGFR phosphorylation (Figure 19D, E).

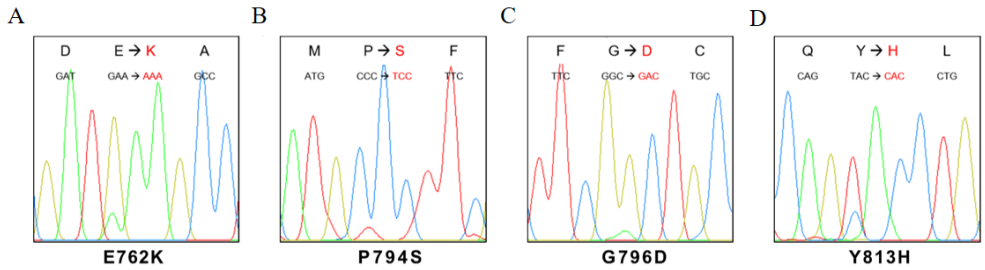

Figure 16. Direct sequencing results of hotspot *EGFR* mutations associated with acquired resistance to osimertinib.

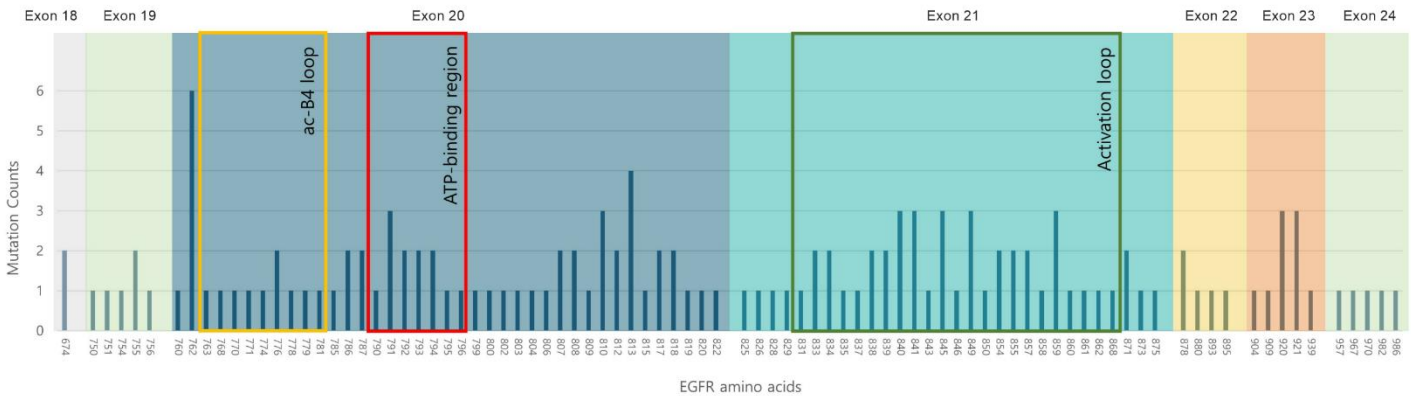

Figure 17. Screened *EGFR* mutations from ENU mutagenesis screening.

Identified mutations were counted and seen as count-hit bars. Distinct structural regions were signed with colored boxes; αC-helix as orange, ATP-binding region as red, and activation loop as green.

Table 6. The list of osimertinib resistant *EGFR* mutations of ENU mutagenesis screening within *EGFR* exon 17 to 25.

#	EGFR site	mutation
1	674	V674A
2	674	V674A
3	750	A750P
4	751	T751P/A/S
5	754	K754I
6	755	A755S/T/P
7	755	A755S/T/P
8	756	N756I
9	760	L760P
10	762	E762K
11	762	E762K
12	762	E762K
13	762	E762A/G/V
14	762	E762K
15	762	E762K
16	763	A763S
17	768	S768C
18	770	D770H/Y
19	771	N771Y
20	774	H insertion --> R
21	776	R776H
22	776	R776C
23	778	L778M
24	779	G779S
25	781	C781F
26	785	T785I
27	786	V786L
28	786	V786M
29	787	Q787P
30	787	Q787H
31	790	T790A
32	791	Q791H
33	791	Q791H
34	791	Q791L
35	792	L792I
36	792	L792I/S
37	793	M793L
38	793	M793L
39	794	P794S
40	794	P794A
41	795	F795L
42	796	G796D
43	799	L799V
44	800	D800C
45	802	V802I
46	803	R803Q
47	804	E804 Stop gain
48	806	K806T
49	807	D807Y
50	807	D807Y
51	808	N808Y
52	808	N808D
53	809	I809S
54	810	G810V
55	810	G810D
56	810	G810V
57	812	Q812H
58	812	Q812H
59	813	Y813H
60	813	Y813H
61	813	Y813 Stop gain
62	813	Y813D
63	815	L815I
64	817	W817C
65	817	W817C
66	818	C818G/S
67	818	C818R/S

68	819	V819R
69	820	Q820H/P
70	822	A822S
71	825	M825T/I
72	826	N826D
73	828	E828D
74	829	E829D
75	831	R831C
76	833	V834G
77	833	L833F
78	834	H835R
79	834	V834M
80	835	H835Q
81	837	D837Y/C
82	838	A839S
83	838	L838Q
84	839	A839P/L
85	839	A839T
86	840	A840S
87	840	A840S
88	840	A840V
89	841	R841W
90	841	R841T
91	841	R841T
92	843	V843L
93	845	V845A
94	845	V845E
95	845	V845L
96	846	K846R/L
97	849	Q849D
98	849	Q849L
99	849	Q849H
100	850	H850Y
101	854	T854S
102	854	T854S
103	855	D855H
104	855	D855H
105	857	G857R
106	857	G857W
107	858	L858M
108	859	A859P/S
109	859	A859P/L
110	859	A859S
111	860	K860N
112	861	L861Q
113	862	L862M
114	868	E868Q
115	871	A871V
116	871	A871V
117	873	G873V
118	875	K875N
119	878	I878V
120	878	I878L
121	880	W880 Stop gain
122	893	H893Q
123	895	S895R
124	904	V904D
125	909	T909K
126	920	A920V
127	920	A920V
128	920	A920D
129	921	S921I
130	921	S921I
131	921	S921R
132	939	V939I
133	957	N957D
134	967	E967K
135	970	K970T/N
136	982	Q982 Stop gain
137	986	D986G

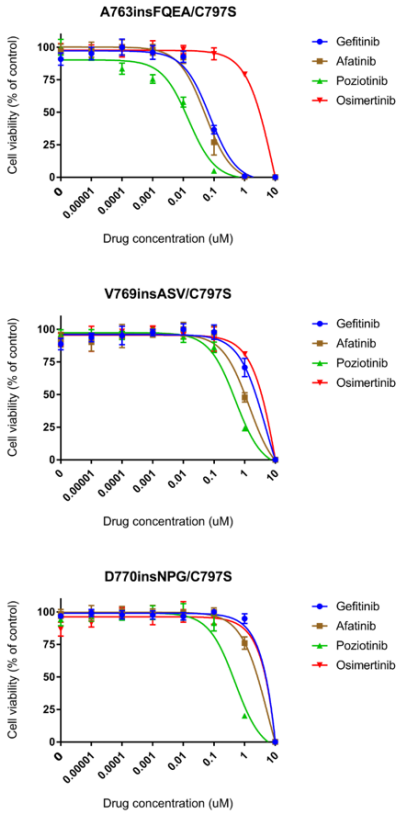

	Gefitinib	Afatinib	Poziotinib	Osimertinib
IC_{50} (nM)	80.75	58.71	12.95	3193.28
S.D.	7.04	14.11	1.66	364.59

	Gefitinib	Afatinib	Poziotinib	Osimertinib
IC_{50} (nM)	2640.7	1108.9	512.5	3964.0
S.D.	547.2	111.5	34.9	485.8

	Gefitinib	Afatinib	Poziotinib	Osimertinib
IC_{50} (nM)	> 5μM	2641.4	508.6	> 5μM
S.D.		534.2	53.8	

Figure 18. Development of *EGFR* C797S positive exon 20 insertion models. Cell viability assays were performed with constructed A763insFQEA/C797S, V769insASV/C797, and D770insNPG/C797S Ba/F3 cells. This cell viability assays were repeated three times independently, and graphs represent mean values with S.D.

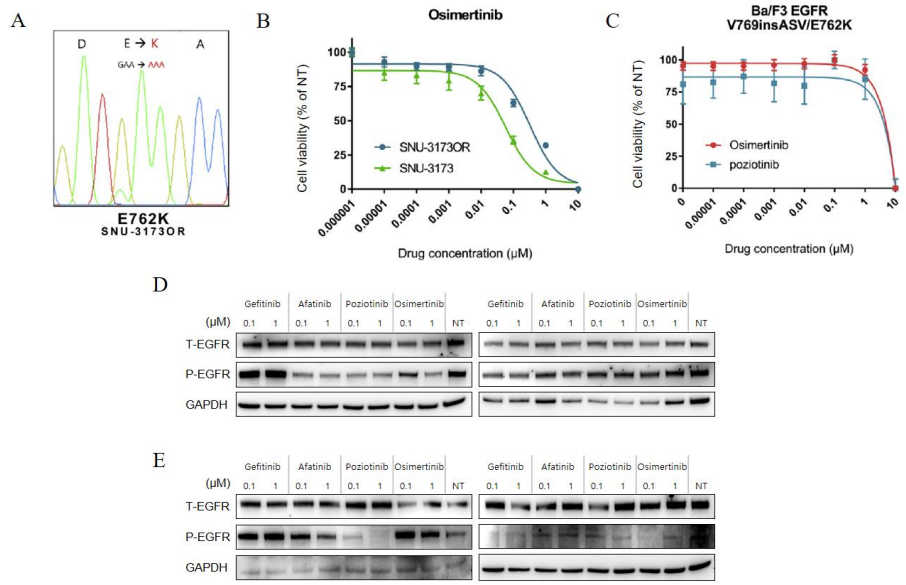

Figure 19. Identification of *EGFR* E762K mutation.

(A) Direct sequencing result of SNU-3173OR cells. (B) Cell viability assay of osimertinib against SNU-3173 and SNU-3173OR cells. (C) Cell viability assay of E762K mutated *EGFR* V769insASV Ba/F3 cells. These cell viability assays were repeated three times independently, and graphs represent mean values with S.D. Immunoblot assay of (D) V769insASV, V769insASV/E762K and (E) H773insH, H773insH/E762K expressing 293T cells. All cells were treated with 100 nM or 1 μM EGFR TKIs for 4 hours. The housekeeping gene GAPDH was used as a loading control.

DISCUSSION

We demonstrated that the 3rd-generation EGFR TKI, osimertinib, showed active inhibitory effect against *EGFR* exon 20 insertion mutant preclinical models and the patient-derived cell line, SNU-3173. Comparing homology models with osimertinib docking simulations, osimertinib can bind into the EGFR D770insNPG mutant drug-binding pocket similarly to EGFR L858R/T790M. Furthermore, among the *EGFR* mutants to wild-type ratios of EGFR TKIs IC_{50} values, osimertinib was significantly lower than the other EGFR TKIs. Regarding osimertinib resistant mechanisms, *EGFR* E762K was the most frequently identified through ENU mutagenesis screening of Ba/F3 cells and also found in SNU-3173OR, osimertinib resistant patient-derived cells.

Except *EGFR* A763insFQEA that was relatively insensitive to the 3rd-generation EGFR TKIs, osimertinib is highly active against the other *EGFR* exon 20 insertion mutant models (Figure 20) [15]. Even though H773insH mutant harboring Ba/F3 cells were mostly insusceptible to EGFR TKIs, showed sensitivity to osimertinib. Several previous studies showed osimertinib efficacy limited to *in vitro* or *in vivo* models using EGFR H773HVdup, H773insNPH, and P773insDNP mutations. However, these models hard to represent all the variations of *EGFR* exon 20 insertions [23, 24]. Latest studies supported our results, the anti-tumor efficacies of osimertinib using *EGFR* D770insSVD and V769insASV harboring NCI-H2073 cells, and other activating insertion in αC-

helix following loop mutations; EGFR D770insG, D770>GY, and N771insN [25-27].

In this study, we developed seven kinds of *EGFR* exon 20 insertion mutant models and SNU-3173 that was derived from a lung adenocarcinoma patient, taking up about 60% of all *EGFR* exon 20 insertion variations in COSMIC database [14]. Our EGFR TKIs screening using eight EGFR exon 20 insertion mutant models is the largest EGFR exon 20 insertion mutant research reveal the anti-tumor effects of osimertinib. Even though poziotinib, a pan-EGFR inhibitor was identified and studied as a potent *EGFR* exon 20 insertion targeting reagent, more than half of patients in clinical trial [NCT03066206] necessarily reduced dose because of side effects related to the inhibition of wild-type *EGFR* (Figure 21) [8]. Additionally, in spite of 55% high objective response rates, median progression free survival was about 5.5 months. Besides, in the latest clinical trial of osimertinib for *EGFR* exon 20 insertion mutant NSCLC [NCT03414814], the patients with longer PFS in the trial include A767insASV (same as V769insASV), and other rare insertions. These osimertinib-affected subtypes cover more than 22% of total *EGFR* exon 20 insertion mutations, and the most frequent V769insASV mutation was sensitive to osimertinib simultaneously in clinical trial and *in vitro* results [28]. These results suggested that alternative therapeutic strategies will be inevitable like afatinib or osimertinib combined with cetuximab or subtype specific treatments for *EGFR* exon 20 insertion mutant NSCLC patients [7, 29, 30]. During this study, the other 3rd-generation EGFR TKI, lazertinib (YH-25448) was

developed which can penetrate BBB. We tested this compound to SNU-3173, and it was insensitive as 587 nM of IC_{50} value (Figure 22). Thus, according to the low mutant to wild-type IC_{50} value ratios of osimertinib, it can be an alternative treatment for *EGFR* exon 20 insertion mutant NSCLCs as a previous case of osimertinib responded to *EGFR* D770insSVD mutation [31].

Due to toxicity and dose affairs, xenograft model developments using SNU-3173 were attempted, however SNU-3173 cells hardly grew in animal models. Alternatively, colony forming assay, *EGFR* wild-type Ba/F3 cells and Calu-3 which have *EGFR/ALK/KRAS* triple-negative lung cancer cells were used for verifying *EGFR* wild-type sparing. These cells showed *EGFR* wild-type sparing with osimertinib in similar level, and *EGFR* mutant to wild-type ratios were shown as subequal manner. However, *EGFR* wild-type inhibitory effects of poziotinib against *EGFR* wild-type Ba/F3 and Calu-3 cells were more sensitive than against other exon 20 insertion mutant cells (Figure 9).

EGFR exon 20 insertion mutations showed sensitivity to osimertinib in functional studies, however it was needed to evaluate with structural evidence. Thus, we constructed several EGFR exon 20 insertion mutant homology models. If EGFR exon 20 inserted amino acids make any folds or curves that push amino acids bilaterally, these irregular structural changes might make the entrance of ATP-binding pocket narrow and lower drug binding affinities. Due to the structural changes as P-loop and αC-helix in crystallization of D770insNPG, EGFR TKIs scarcely bind into drug-binding pocket

appropriately [8, 9]. However, docking simulations of homology models in this study showed that osimertinib could bind to D770insNPG as similar manner with EGFR L858R/T790M. Additionally, according to comparing cell viability assay and docking simulation with osimertinib among *EGFR* mutant models, IC_{50} values and delta G values were moderately correlated.

Because of unavoidable acquired resistance, we identified osimertinib-resistant mechanisms against *EGFR* exon 20 insertion mutant Ba/F3 cells using ENU mutagenesis screening. Various and numerous mutations were identified, especially mutations occurred on E762 and Y813 had multiple hits. EGFR E762 located before the insertion mutations and well-conserved in αC-helix of EGFR N-lobe. E762 forms a salt bridge with K745 and this interaction mediates the structural changes between EGFR active form (αC-in motif) and inactive form (αC-out motif) [32]. In the screening, E762K mutation detected most frequently, and this mutation was not observed in NSCLC before, but in sporadic breast cancer [16, 33]. In our study, we identified this mutation that is resistant to not only osimertinib, but also poziotinib (Figure 19B). Previous studies revealed that salt bridge conformation of E762-K745 is indispensable for catalytic activity within αC-helix-in and -out motif [15, 26, 34, 35]. However, it is unknown how the E762K mutation mediates EGFR TKIs resistance. Via EGFR homology models, we modeled what glutamic acid (E) can interact with K745 for EGFR activation when the E762K mutation arose (Figure 23). Before 762 toward N-terminus in the αC-helix, E758 is the nearest glutamic acid which possibly interact with K745. During conforming E758-K745 bridge, E762K

can interact with the other residue. However, what amino acids will interact with E762K mutation is unknown. To reveal the interactions and effects of *EGFR* exon 20 insertions with E762K as the resistant mechanism, it is needed to study exon 20 insertion mutant EGFR structure in depth.

Even we revealed various osimertinib-resistant mutations, the well-known osimertinib resistant mechanism C797S was not identified. However, several known osimertinib-resistant mutations as *EGFR* P794S and G796D near C797 were observed in this screening assay [16, 17]. Although ENU mutagenesis screening of *EGFR* mutant Ba/F3 cells was limited just in *EGFR*, those diverse and abundant mutations on *EGFR* might restrain the long-term usage of EGFR TKIs.

In conclusion, we demonstrated osimertinib efficacy against *EGFR* exon 20 insertion mutant cells with superior wild-type *EGFR* sparing. Moreover, in the homology models and docking simulations of osimertinib with *EGFR* exon 20 insertion mutants, osimertinib flexibly binds into the drug-binding sites. Numerous *EGFR* mutations which are resistant to osimertinib were observed through ENU mutagenesis screening of *EGFR* exon 20 insertion mutant Ba/F3 cells. Especially, E762K that was substituted from catalytically indispensable glutamic acids on 762 was identified in ENU mutagenesis screening and SNU-3173OR cells coincidentally. This study has led to the launch of a phase II clinical trial of osimertinib dose at 80 mg once daily [NCT03414814] for *EGFR* exon 20 insertion mutant NSCLC patients in Korea. Furthermore, these results support the ongoing phase II clinical trial of osimertinib in western with higher

dose at 160 mg once daily for *EGFR* exon 20 insertion mutant NSCLC patients. The ORR of osimertinib was 6% for EGFR exon 20 insertion mutant NSCLC in retrospective study, however, clinical outcomes of prospective trials might lead to a mutation subtype-specific approach for treating NSCLC patients with *EGFR* exon 20 insertion mutation similar to our variable *in vitro* efficacies of osimertinib [36].

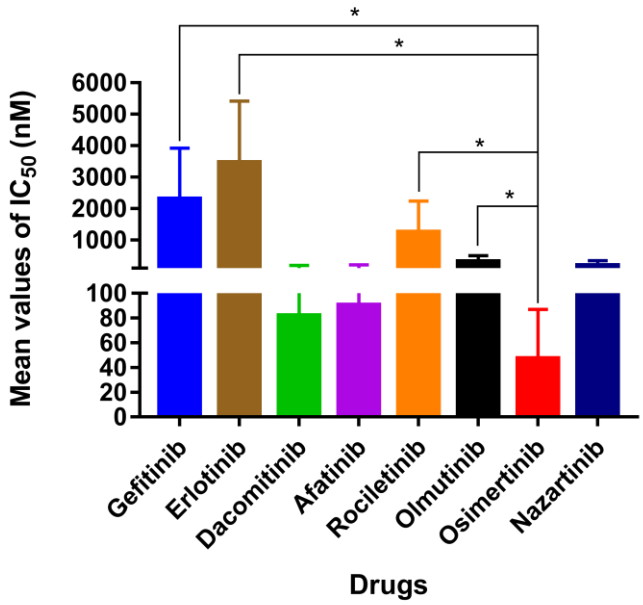

Figure 20. One-way ANOVA comparisons of EGFR TKIs.

Each bar indicates mean values of each EGFR TKI IC_{50} values against *EGFR* exon 20 insertion mutant cells. Statistical significances of osimertinib comparing to the other EGFR TKIs were indicated with an asterisk at $P<0.05$.

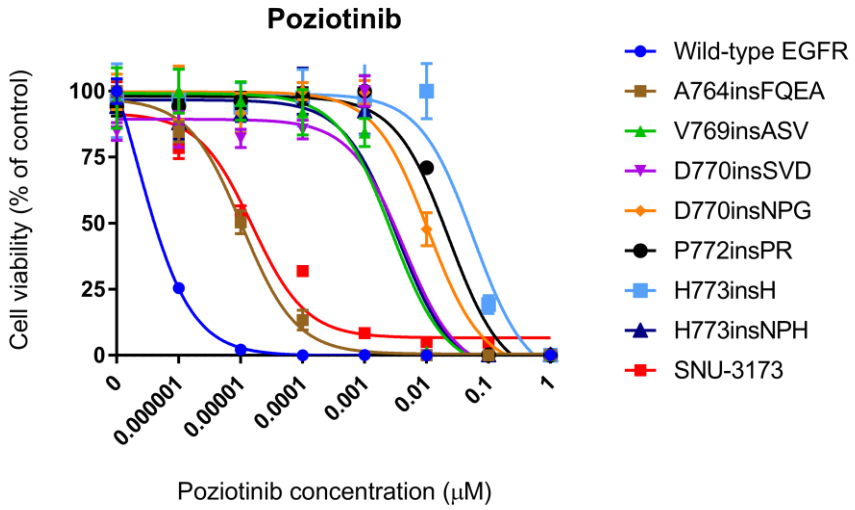

IC_{50}(nM)	WT (+EGF 30ng/mL)	FQEA	ASV	SVD	NPG	PR	H	NPH	SNU-3173
Mean	0.000512	0.0101	2.87	4.05	10.04	22.80	51.34	3.37	0.023

Figure 21. Efficacy of poziotinib against *EGFR* exon 20 insertion mutant cells.

All *EGFR* exon 20 insertion mutant Ba/F3 and SNU-3173 cells were exposed to poziotinib for 72 hours. These experiments were repeated three times independently, and graphs represent mean ± S.D. values.

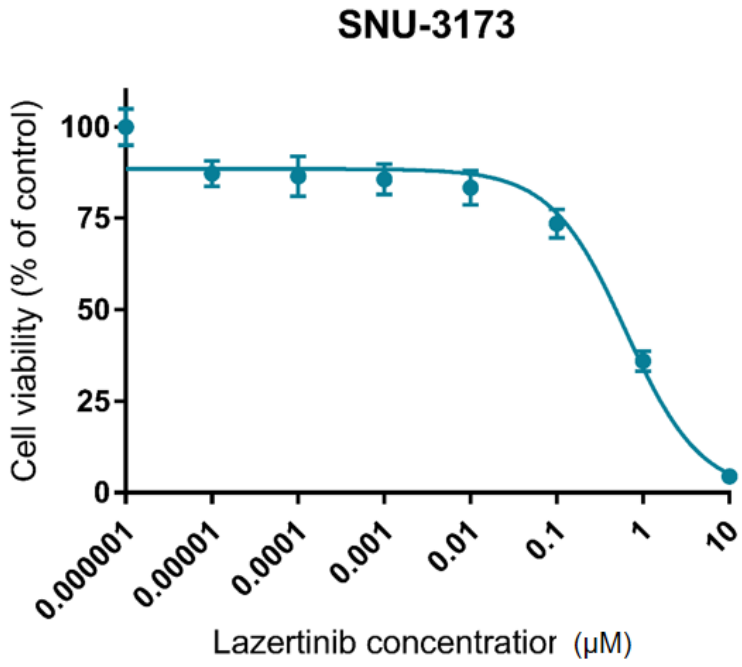

Figure 22. Cell viability assay of lazertinib (YH-25448) against SNU-3173. SNU-3173 cells were exposed to lazertinib for 72 hours and analyzed IC_{50} value is 587.02 nM. These experiments were repeated three times independently, and graphs represent mean ± S.D. values.

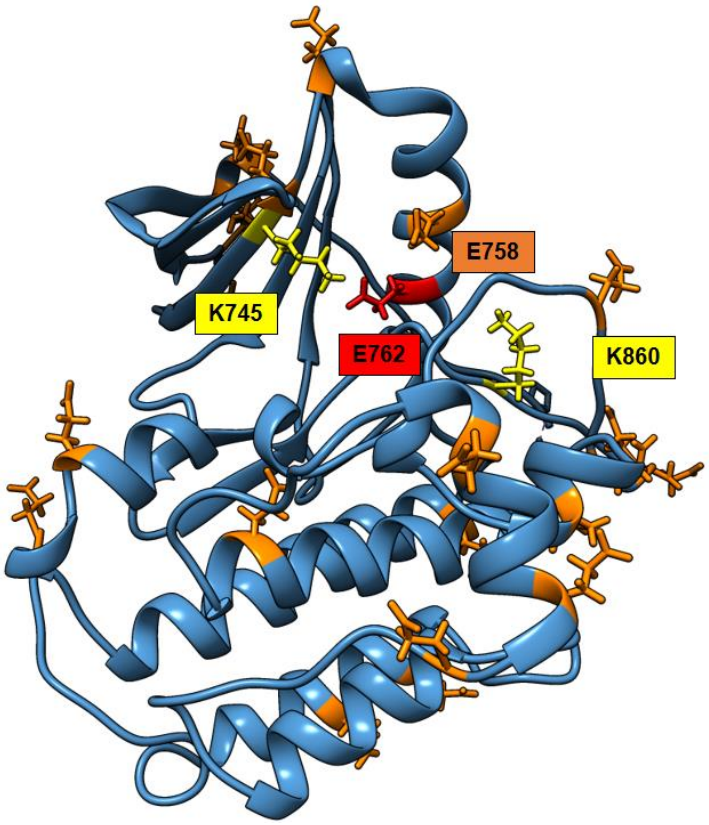

Figure 23. The homology model of active EGFR.

Salt bridge conformation residues E762 and K745 colored with red and yellow, respectively, and K860 that also interact with E762 in the inactive form wild-type EGFR (PDB ID: 4ZAU). All glutamic acids (E) except E762 were colored by orange.

REFERENCE

1. R. L. Siegel, K. D. Miller, and A. Jemal, *Cancer statistics, 2018.* CA Cancer J Clin, 2018. **68**(1): p. 7-30.
2. A. Shin, C.-M. Oh, B.-W. Kim, H. Woo, Y.-J. Won, and J.-S. Lee, *Lung cancer epidemiology in Korea.* Cancer research and treatment: official journal of Korean Cancer Association, 2017. **49**(3): p. 616.
3. R. S. Herbst, D. Morgensztern, and C. Boshoff, *The biology and management of non-small cell lung cancer.* Nature, 2018. **553**(7689): p. 446.
4. J.-S. Seo, Y. S. Ju, W.-C. Lee, J.-Y. Shin, J. K. Lee, T. Bleazard, J. Lee, Y. J. Jung, J.-O. Kim, and J.-Y. Shin, *The transcriptional landscape and mutational profile of lung adenocarcinoma.* Genome research, 2012. **22**(11): p. 2109-2119.
5. C. R. Chong and P. A. Janne, *The quest to overcome resistance to EGFR-targeted therapies in cancer.* Nat Med, 2013. **19**(11): p. 1389-1400.
6. H. Yasuda, S. Kobayashi, and D. B. Costa, *EGFR exon 20 insertion mutations in non-small-cell lung cancer: preclinical data and clinical implications.* The Lancet Oncology, 2012. **13**(1): p. e23-e31.
7. J. C.-H. Yang, Y.-L. Wu, M. Schuler, M. Sebastian, S. Popat, N. Yamamoto, C. Zhou, C.-P. Hu, K. O'Byrne, and J. Feng, *Afatinib versus cisplatin-based chemotherapy for EGFR mutation-positive lung adenocarcinoma (LUX-Lung 3 and LUX-Lung 6): analysis of overall*

survival data from two randomised, phase 3 trials. The Lancet Oncology, 2015. **16**(2): p. 141-151.

8. J. P. Robichaux, Y. Y. Elamin, Z. Tan, B. W. Carter, S. Zhang, S. Liu, S. Li, T. Chen, A. Poteete, A. Estrada-Bernal, A. T. Le, A. Truini, M. B. Nilsson, H. Sun, E. Roarty, S. B. Goldberg, J. R. Brahmer, M. Altan, C. Lu, V. Papadimitrakopoulou, K. Politi, R. C. Doebele, K. K. Wong, and J. V. Heymach, *Mechanisms and clinical activity of an EGFR and HER2 exon 20-selective kinase inhibitor in non-small cell lung cancer.* Nat Med, 2018. **24**(5): p. 638-646.

9. J. Heymach, M. Negrao, J. Robichaux, B. Carter, A. Patel, M. Altan, D. Gibbons, F. Fossella, G. Simon, V. Lam, G. Blumenschein, A. Tsao, J. Kurie, F. Mott, D. Jenkins, D. Mack, L. Feng, B. Roeck, Z. Yang, V. Papadimitrakopoulou, and Y. Elamin, *OA02.06 A Phase II Trial of Poziotinib in EGFR and HER2 exon 20 Mutant Non-Small Cell Lung Cancer (NSCLC).* Journal of Thoracic Oncology, 2018. **13**(10): p. S323-S324.

10. H. Greulich, T. H. Chen, W. Feng, P. A. Janne, J. V. Alvarez, M. Zappaterra, S. E. Bulmer, D. A. Frank, W. C. Hahn, W. R. Sellers, and M. Meyerson, *Oncogenic transformation by inhibitor-sensitive and -resistant EGFR mutants.* PLoS Med, 2005. **2**(11): p. e313.

11. A. Waterhouse, M. Bertoni, S. Bienert, G. Studer, G. Tauriello, R. Gumienny, F. T. Heer, T. A. P. de Beer, C. Rempfer, and L. Bordoli, *SWISS-MODEL: homology modelling of protein structures and complexes.* Nucleic acids research, 2018. **46**(W1): p. W296-W303.

12. A. Grosdidier, V. Zoete, and O. Michielin, *SwissDock, a protein-small molecule docking web service based on EADock DSS.* Nucleic acids research, 2011. **39**(suppl_2): p. W270-W277.

13. E. F. Pettersen, T. D. Goddard, C. C. Huang, G. S. Couch, D. M. Greenblatt, E. C. Meng, and T. E. Ferrin, *UCSF Chimera—a visualization system for exploratory research and analysis.* Journal of computational chemistry, 2004. **25**(13): p. 1605-1612.

14. Z. Sondka, S. Bamford, C. G. Cole, S. A. Ward, I. Dunham, and S. A. Forbes, *The COSMIC Cancer Gene Census: describing genetic dysfunction across all human cancers.* Nature Reviews Cancer, 2018: p. 1.

15. H. Yasuda, E. Park, C. H. Yun, N. J. Sng, A. R. Lucena-Araujo, W. L. Yeo, M. S. Huberman, D. W. Cohen, S. Nakayama, K. Ishioka, N. Yamaguchi, M. Hanna, G. R. Oxnard, C. S. Lathan, T. Moran, L. V. Sequist, J. E. Chaft, G. J. Riely, M. E. Arcila, R. A. Soo, M. Meyerson, M. J. Eck, S. S. Kobayashi, and D. B. Costa, *Structural, biochemical, and clinical characterization of epidermal growth factor receptor (EGFR) exon 20 insertion mutations in lung cancer.* Sci Transl Med, 2013. **5**(216): p. 216ra177.

16. F. Martínez-Jiménez, J. P. Overington, B. Al-Lazikani, and M. A. Marti-Renom, *Rational design of non-resistant targeted cancer therapies.* Scientific reports, 2017. **7**: p. 46632.

17. S. J. Klempner, P. Mehta, A. B. Schrock, S. M. Ali, and S.-H. I. Ou, *Cis-oriented solvent-front EGFR G796S mutation in tissue and ctDNA*

in a patient progressing on osimertinib: a case report and review of the literature. Lung Cancer: Targets and Therapy, 2017. **8**: p. 241.

18. D. Zheng, M. Hu, Y. Bai, X. Zhu, X. Lu, C. Wu, J. Wang, L. Liu, Z. Wang, and J. Ni, *EGFR G796D mutation mediates resistance to osimertinib.* Oncotarget, 2017. **8**(30): p. 49671.

19. K. S. Thress, C. P. Paweletz, E. Felip, B. C. Cho, D. Stetson, B. Dougherty, Z. Lai, A. Markovets, A. Vivancos, Y. Kuang, D. Ercan, S. E. Matthews, M. Cantarini, J. C. Barrett, P. A. Janne, and G. R. Oxnard, *Acquired EGFR C797S mutation mediates resistance to AZD9291 in non-small cell lung cancer harboring EGFR T790M.* Nat Med, 2015. **21**(6): p. 560-562.

20. X. Le, S. Puri, M. V. Negrao, M. B. Nilsson, J. Robichaux, T. Boyle, J. K. Hicks, K. L. Lovinger, E. Roarty, and W. Rinsurongkawong, *Landscape of EGFR-dependent and-independent resistance mechanisms to osimertinib and continuation therapy beyond progression in EGFR-mutant NSCLC.* Clinical Cancer Research, 2018. **24**(24): p. 6195-6203.

21. Z. Yang, N. Yang, Q. Ou, Y. Xiang, T. Jiang, X. Wu, H. Bao, X. Tong, X. Wang, Y. W. Shao, Y. Liu, Y. Wang, and C. Zhou, *Investigating Novel Resistance Mechanisms to Third-Generation EGFR Tyrosine Kinase Inhibitor Osimertinib in Non-Small Cell Lung Cancer Patients.* Clin Cancer Res, 2018. **24**(13): p. 3097-3107.

22. S. I. Ou, J. Cui, A. B. Schrock, M. E. Goldberg, V. W. Zhu, L. Albacker, P. J. Stephens, V. A. Miller, and S. M. Ali, *Emergence of novel and*

dominant acquired EGFR solvent-front mutations at Gly796 (G796S/R) together with C797S/R and L792F/H mutations in one EGFR (L858R/T790M) NSCLC patient who progressed on osimertinib. Lung Cancer, 2017. **108**: p. 228-231.

23. D. A. Cross, S. E. Ashton, S. Ghiorghiu, C. Eberlein, C. A. Nebhan, P. J. Spitzler, J. P. Orme, M. R. Finlay, R. A. Ward, M. J. Mellor, G. Hughes, A. Rahi, V. N. Jacobs, M. Red Brewer, E. Ichihara, J. Sun, H. Jin, P. Ballard, K. Al-Kadhimi, R. Rowlinson, T. Klinowska, G. H. Richmond, M. Cantarini, D. W. Kim, M. R. Ranson, and W. Pao, *AZD9291, an irreversible EGFR TKI, overcomes T790M-mediated resistance to EGFR inhibitors in lung cancer.* Cancer Discov, 2014. **4**(9): p. 1046-1061.

24. M. Yang, X. Xu, J. Cai, J. Ning, J. P. Wery, and Q. X. Li, *NSCLC harboring EGFR exon-20 insertions after the regulatory C-helix of kinase domain responds poorly to known EGFR inhibitors.* Int J Cancer, 2016. **139**(1): p. 171-176.

25. N. Floc'h, M. J. Martin, J. W. Riess, J. P. Orme, A. D. Staniszewska, L. Menard, M. E. Cuomo, D. J. O'Neill, R. A. Ward, M. R. V. Finlay, D. McKerrecher, M. Cheng, D. P. Vang, R. A. Burich, J. G. Keck, D. R. Gandara, P. C. Mack, and D. A. E. Cross, *Antitumor Activity of Osimertinib, an Irreversible Mutant-Selective EGFR Tyrosine Kinase Inhibitor, in NSCLC Harboring EGFR Exon 20 Insertions.* Mol Cancer Ther, 2018. **17**(5): p. 885-896.

26. Z. Ruan and N. Kannan, *Altered conformational landscape and dimerization dependency underpins the activation of EGFR by alphaC-beta4 loop insertion mutations.* Proc Natl Acad Sci U S A, 2018. **115**(35): p. E8162-E8171.

27. W. Fang, Y. Huang, S. Hong, Z. Zhang, M. Wang, J. Gan, W. Wang, H. Guo, K. Wang, and L. Zhang, *EGFR exon 20 insertion mutations and response to osimertinib in non-small-cell lung cancer*. BMC Cancer, 2019. **19**(1): p. 595.

28. T. M. Kim, C.-Y. Ock, M. Kim, S. H. Kim, B. Keam, Y. J. Kim, D.-W. Kim, J.-S. Lee, and D. S. Heo, *1529PPhase II study of osimertinib in NSCLC patients with EGFR exon 20 insertion mutation: A multicenter trial of the Korean Cancer Study Group (LU17-19).* Annals of Oncology, 2019. **30**(Supplement_5).

29. H. Hasegawa, H. Yasuda, J. Hamamoto, K. Masuzawa, T. Tani, S. Nukaga, T. Hirano, K. Kobayashi, T. Manabe, H. Terai, S. Ikemura, I. Kawada, K. Naoki, and K. Soejima, *Efficacy of afatinib or osimertinib plus cetuximab combination therapy for non-small-cell lung cancer with EGFR exon 20 insertion mutations.* Lung Cancer, 2019. **127**: p. 146-152.

30. W. Fang, Y. Huang, J. Gan, Y. W. Shao, and L. Zhang, *Durable Response of Low-Dose Afatinib plus Cetuximab in an Adenocarcinoma Patient with a Novel EGFR Exon 20 Insertion Mutation.* J Thorac Oncol, 2019. **14**(10): p. e220-e221.

31. Z. Piotrowska, F. J. Fintelmann, L. V. Sequist, and B. Jahagirdar, *Response to Osimertinib in an EGFR exon 20 insertion-positive lung adenocarcinoma.* Journal of Thoracic Oncology, 2018. **13**(10): p. e204-e206.

32. Y. Shan, M. P. Eastwood, X. Zhang, E. T. Kim, A. Arkhipov, R. O. Dror, J. Jumper, J. Kuriyan, and D. E. Shaw, *Oncogenic mutations counteract intrinsic disorder in the EGFR kinase and promote receptor dimerization.* Cell, 2012. **149**(4): p. 860-870.

33. F. Weber, K. Fukino, T. Sawada, N. Williams, K. Sweet, R. Brena, C. Plass, T. Caldes, G. Mutter, and M. Villalona-Calero, *Variability in organ-specific EGFR mutational spectra in tumour epithelium and stroma may be the biological basis for differential responses to tyrosine kinase inhibitors.* British journal of cancer, 2005. **92**(10): p. 1922.

34. S. Ikemura, H. Yasuda, S. Matsumoto, M. Kamada, J. Hamamoto, K. Masuzawa, K. Kobayashi, T. Manabe, D. Arai, I. Nakachi, I. Kawada, K. Ishioka, M. Nakamura, H. Namkoong, K. Naoki, F. Ono, M. Araki, R. Kanada, B. Ma, Y. Hayashi, S. Mimaki, K. Yoh, S. S. Kobayashi, T. Kohno, Y. Okuno, K. Goto, K. Tsuchihara, and K. Soejima, *Molecular dynamics simulation-guided drug sensitivity prediction for lung cancer with rare EGFR mutations.* Proc Natl Acad Sci U S A, 2019. **116**(20): p. 10025-10030.

35. J. Niggenaber, J. Hardick, J. Lategahn, and D. Rauh, *Structure Defines Function: Clinically Relevant Mutations in ErbB Kinases.* J Med Chem, 2019.

36. B. van Veggel, A. van der Wekken, S. Hashemi, R. Cornelissen, K. Monkhorst, D. Heideman, T. Radonic, E. Smit, E. Schuuring, and J. De Langen, *1450P Osimertinib treatment for patients with EGFR exon 20 insertion positive non-small cell lung cancer.* Annals of Oncology, 2018. **29**(suppl_8): p. mdy292. 072.

국문초록

연구 목적: 상피 성장인자 수용체(Epidermal Growth Factor Receptor, *EGFR*) 엑손 20 삽입 돌연변이가 있는 비소세포폐암은 상피 성장인자 수용체 돌연변이 비소세포폐암에서 3 번째로 높은 발병률을 보인다. 본 연구에서는 상피 성장인자 수용체 엑손 20 삽입 돌연변이의 전임상 모델들을 구축하고, 또한 해당 모델들에 대한 1, 2, 그리고 3 세대 상피 성장인자 수용체 티로신 키나아제 억제제의 효능을 확인하고자 하였다.

연구 방법: 본 연구에서는 부위 유도 돌연변이 기법을 통하여 상피 성장인자 수용체 엑손 20 삽입 돌연변이인 A763insFQEA, V769insASV, D770insSVD, D770insNPG, P772insPR, H773insH, H773insNPH 를 발현하는 Ba/F3 세포주 모델과, 또한 H773insAH 돌연변이를 가진 환자 유래 세포주 (SNU-3173)를 구축하였다. 해당 전임상 모델들을 사용하여 세포 생활력 분석법, 면역탁본 분석법, 그리고 N-Ethyl-N-nitrosourea (ENU) 돌연변이 유발 검사법을 진행하였고, 상피 성장인자 수용체 엑손 20 삽입 돌연변이 구조체와 3 세대 상피 성장인자 수용체 티로신 키나아제 억제제인 osimertinib 과의 결합 모델을 구축하고 비교하였다.

연구 결과: A763insFQEA 돌연변이를 제외한 상피 성장인자 수용체 엑손 20 삽입 돌연변이 세포들은 1 세대 상피 성장인자 수용체 티로신 키나아제 억제제에 대하여 내성을 보였다 (IC_{50}, 1.1±0.067 ~ 5.4±0.115 μM). 2 세대 상피 성장인자 수용체 티로신 키나아제 억제제들은 대부분의 돌연변이들에 대하여 민감성을 보였지만 (IC_{50}, 0.02±0.0002 ~ 161.8±18.7nM), H773insH 돌연변이는 비교적 덜 민감한 결과를 보였다 (IC_{50}, 46.3±8.0 ~ 352.5±22.7nM). 2 세대 상피 성장인자 수용체 티로신 키나아제 억제제의 야생형에 대한 돌연변이의 IC_{50} 비율은 3 세대 티로신 키나아제 억제제들보다 높게 나타났다. 3 세대 상피 성장인자 수용체 티로신 키나아제 억제제인 osimertinib 은 H773insH 돌연변이를 포함하는 모든 상피 성장인자 수용체 엑손 20 삽입 돌연변이에 대하여 좋은 효과를 보였고 (IC_{50}, 14.7 ~ 62.7nM), 야생형 상피 성장인자 수용체를 잘 보존할 수 있었다. 상피 성장인자 수용체 엑손 20 삽입 돌연변이 상동성 모형화와 도킹 모의실험을 통하여 osimertinib 이 약제 결합 부위에 유연하게 결합하는 양상을 확인할 수 있었다. 또한, 상피 성장인자 수용체 엑손 20 삽입 돌연변이 Ba/F3 세포들에 대하여 ENU 돌연변이 유발 검사법을 진행한 결과, 상피 성장인자 수용체의 다양한 부위에서 돌연변이를 보였고, E762K, P794S, 그리고 G796D 돌연변이를 포함하는 엑손 20 과 21 에서 대부분 발생하였다. 더불어, 단계별 약제 농도 노출을 통한 osimertinib 내성 SNU-3173 세포주를 구축하였고, ENU 돌연변이

유발 검사법에서 발생한 상피 성장인자 수용체 E762K 돌연변이가 동일하게 확인되었다. 또한, 해당 돌연변이에 대한 기능적 연구를 통하여 상피 성장인자 수용체 티로신 키나아제 억제제의 내성기전으로 작용함을 확인하였다.

결론: Osimertinib 은 상피 성장인자 수용체 엑손 20 삽입 돌연변이에 대하여 활성을 보이고, 약물 결합 부위에 유연하게 결합한다.

주요어: 비소세포폐암, EGFR, 엑손 20 삽입, 내성, osimertinib

학번: 2015-22059

ACKNOWLEDGEMENT

I express my deep gratitude for those who have helped me finalize my dissertation study. Dae Seog Heo and Dong-Wan Kim supervised this research and helped the interpretation of data. Tae Min Kim helped experimental design and supplied clinical samples and data. Bhumsuk Keam and Miso Kim contributed to data interpretation. Soyeon Kim conceived and contributed *in vitro* experiments. Ja-Lok Ku developed the patient-derived cell line, SNU-3173. All the authors above contributed to the research.

This work was supported by Korean Foundation for Cancer Research (KFCR-2017-004).